Parameter Estimation of PMSMs Without Signal Injection and Dedicated Tests Considering Voltage Errors and Parameter Variations

Elia Brescia, Luigi Pio Savastio, *Graduate Student Member, IEEE*, Mauro Di Nardo, *Member, IEEE*, Giuseppe Leonardo Cascella, *Member, IEEE*, and Francesco Cupertino, *Senior Member, IEEE*

***Abstract*—This article proposes an offline noninvasive method for the parameter estimation of permanent magnet synchronous motors controlled with nonzero d-axis current. The proposed algorithm has been specifically designed to operate in application scenarios, where custom signal injection and dedicated test campaigns are not possible and are potentially characterized by scarce measurement data variety. The rank deficiency issue that affects the parameter estimation has been addressed by exploiting data measurements from two different speed/load motor operating conditions (OCs). When more than two OCs are available, the ones used for the parameter estimation are automatically selected to mitigate the estimation errors caused by imperfect inverter nonlinearity compensation and parameter variations. The proposed method has been validated and compared with existing noninvasive parameter estimation approaches on experimental datasets collected from two different motors. The results show that the proposed methodology outperforms existing approaches in scenarios characterized by scarce variety of available motor OCs, ensuring moderate estimation errors.**

***Index Terms*—Inverter nonlinearity, magnetic saturation, parameter estimation, permanent magnet synchronous machines (PMSMs), rank deficiency.**

I. Introduction

PERMANENT magnet synchronous motors are used in a wide variety of applications, such as renewable energy, microgrids, aerospace, and traction [1], [2], [3], [4]. Estimating the parameters of permanent magnet synchronous motors (PMSMs) is useful to improve the dynamic performance and efficiency of the drive control system, to implement sensorless and robust control techniques, and for condition monitoring and fault diagnosis [5], [6], [7]. The methodologies proposed for the parameter estimation of PMSMs can be categorized into online and offline approaches.

Online approaches are based on algorithms executed in real time by the drive control unit during motor operation. This approach suffers from the well-known issue of rank deficiency, since the number of unknown parameters is higher than the rank of the mathematical model of the PMSM [8], [9], [10]. To overcome this issue in online approaches, two main solutions have been proposed. The first one is based on fixing some parameters to their nominal values or offline measurements to reduce the number of unknown parameters and match the rank of the PMSM model [5], [6], [11], [12], [13], [14]. This approach has been recently adopted, for instance, in [11] and [14]. In particular, Lian et al.[11] proposed the estimation of the stator resistance and rotor flux linkage using a recursive least squares (RLS) algorithm assisted by previous offline estimations of the inductances. Similarly, Li and Kennel[14] achieves a decoupled estimation of the stator resistance and rotor flux linkage using a dual extended Kalman filter by setting the inductances to their offline measurements. Even if this approach is simple and noninvasive, its accuracy is compromised by errors induced by variations of the actual parameters as a function of the motor operating conditions (OCs) [12]. An alternative solution is based on the injection of disturbance signals to obtain measurement data in perturbed OCs of the motor. In this manner, extra equations for the perturbed OCs can be used to increase the rank of the problem, matching the number of unknown parameters. The main proposed methodologies are based on the injection of high-frequency currents or voltages [8], [15], [16], [17], [18], constant d-axis current pulses [9], [10], [19], [20], [21], and rotor position offsets [22], [23], [24]. With respect to the first approach, techniques based on signal injection ensure higher accuracy but require more complex algorithms and affect motor performance by reducing efficiency and increasing torque and speed oscillations [12].

Offline techniques, on the other hand, conventionally rely on dedicated motor tests to collect data that will be processed once the tests are completed. For instance, in [25] and [26], the stator resistance and inductances are estimated through the injection of dc and high-frequency dq-axis currents with the

Received 18 March 2025; revised 29 July 2025 and 15 September 2025; accepted 5 October 2025. Date of publication 8 October 2025; date of current version 13 November 2025. This work was supported in part by Project PE0000021, "Network 4 Energy Sustainable Transition - NEST," funded by the European Union - NextGenerationEU, under the National Recovery and Resilience Plan (NRRP), Mission 4 Component 2 Investment 1.3 - Call for tender No. 1561 of 11.10.2022 of Ministero dell' Università e della Ricerca (MUR) (CUP C93C22005230007), and in part by project "HERMES - H2: Energy vector for Railways transportation; hoMologation, Environment, and Safety" - Bando: Flagship 2024 - LINE B - 2° edition - Projects for research infrastructures and disruptive initiatives. Recommended for publication by Associate Editor T. Shi. *(Corresponding author: Elia Brescia.)*

The authors are with the Department of Electrical and Information Engineering, Politecnico di Bari, 70126 Bari, Italy (e-mail: elia.brescia@poliba.it; l.savastio@phd.poliba.it; mauro.dinardo@poliba.it; giuseppeleonardo.cascella@poliba.it; francesco.cupertino@poliba.it).

Color versions of one or more figures in this article are available at https://doi.org/10.1109/TPEL.2025.3619414.

Digital Object Identifier 10.1109/TPEL.2025.3619414

motor at standstill. In [27] and [28], the motor parameters are estimated after the collection of measurement data under several tests at predefined speed and load OCs. While ensuring high accuracy, offline approaches generally require time-consuming tests, motor downtimes, specialized laboratory setups, and human expertise.

Unfortunately, in real-world applications, the execution of dedicated tests in operational environments or the implementation of custom signal injections and online algorithms in standard off-the-shelf drives is rarely possible. As a result, in most practical circumstances, the only way to estimate the motor parameters is by leveraging measurement data gathered during normal on-load motor operations. Nowadays, the latest generations of electric drives offer the connectivity capability required to transfer massive amounts of data at high sampling rates, which may be automatically collected and processed thanks to modern edge/cloud computing technologies [29]. As a result, it is technologically feasible to handle the parameter estimation of PMSMs in a noninvasive and large-scale manner. However, from a theoretical standpoint, addressing parameter estimation of PMSMs in such settings presents new challenges. In fact, parameter estimation might be undertaken in scenarios potentially characterized by scarce diversity of data and OCs. For instance, typical and widespread scenarios characterized by data scarcity are those where PMSMs are embedded in machines executing periodic work cycles, such as industrial robotic arms in automated production lines or belt conveyors in material-handling systems. Additional examples include fan motors and compressors, which also operate under discrete, repetitive conditions. Moreover, since in such contexts the OCs cannot be selected beforehand, parameter variations are uncontrolled and may negatively impact estimation accuracy. To deal with these issues, in [30] and [31], novel noninvasive approaches relying only on two different motor OCs have been proposed. In cases where more than two OCs are available, an algorithm, supported by an error analysis, has been designed to select the two OCs that minimize estimation errors caused by parameter variations and voltage distortions. The algorithm also allows automatic detection and rejection of estimations potentially affected by excessive estimation errors. These solutions have been specifically designed for PMSMs controlled with zero d-axis current, which is the typical case of isotropic machines in the constant torque region. For these motors, only the estimation of the stator resistance and rotor flux linkage is affected by the rank deficiency issue. However, nonisotropic or isotropic PMSMs operating in the constant power region are typically controlled with a negative d-axis current, which causes the rank deficiency issue also when estimating the stator inductances.

The primary objective of this study is the design of a novel offline noninvasive parameter estimation method for PMSMs controlled with nonzero d-axis current, suitable for scenarios where dedicated tests and signal injections are not possible. In such contexts, the estimated parameters may be highly beneficial, particularly, but not exclusively, for fault diagnosis, condition monitoring, and predictive maintenance. In the first step of the proposed algorithm, the voltage-source-inverter (VSI) nonlinearity is compensated using data collected from a single OC. In the second step, the algorithm estimates the q-axis stator inductance and the stator resistance. The d-axis stator inductance and the rotor flux linkage are estimated in the last step of the algorithm. To solve the rank-deficiency issue in the second and third steps, data collected from two different OCs are simultaneously exploited and automatically selected to mitigate estimation errors caused by parameter variations and voltage errors. Compared to the existing literature, the main contributions of this article can be summarized as follows.

1) Compared to the method of the fixed parameter (FP) (see[5], [6], [11], [12], [13], [14]), the proposed approach considers and mitigates the impact of parameter variations on estimation accuracy.
2) Unlike [8], [9], [10], [15], [16], [19], [22], [23], [24], the proposed approach estimates the PMSM parameters without custom signal injection procedures, which may affect motor performance and are rarely implementable in standard off-the-shelf drives.
3) Differently from offline methods in [25], [27], [28], the proposed approach does not require the execution of dedicated tests on the motor, which necessitate machine downtimes, specialized laboratory setups, and human expertise.
4) In contrast to existing online and offline estimation methods, the proposed approach is specifically designed to estimate the PMSM parameters by exploiting datasets potentially affected by scarce OC variety and availability.
5) Distinct from [30] and [31], this work deals with PMSMs controlled with nonzero d-axis current, addressing the rank-deficient estimation of stator inductances and accounting for magnetic self- and cross-saturation effects.

The rest of this article is organized as follows. Section II describes the model of the PMSM considering the VSI nonlinearity, digital-delay effects, and parameter variations; Section III details the proposed parameter estimation method, while Section IV outlines the procedure for selecting the best OCs for parameter estimation. Section V reports the experimental validation and the comparison of estimation performance with existing noninvasive parameter estimation methods. Finally, Section VI concludes this article.

II. PMSM Model

The proposed parameter estimation method is based on the following discrete-time stationary model of the PMSM, including the voltage distortion caused by the VSI nonlinearity and digital-delay effects

$$\breve{u}_d(k) = Ri_d(k) - L_q\omega(k)i_q(k) - D_d(k)V_{\text{dead}} \quad (1)$$

$$\breve{u}_q(k) = Ri_q(k) + L_d\omega(k)i_d(k) + \psi\omega(k) - D_q(k)V_{\text{dead}} \quad (2)$$

where k is the sampling index, ω is the electrical rotor speed, i_d and i_q are the dq-axes currents, D_d and D_q are the VSI distorted coefficients [11], V_{dead} is the VSI distorted voltage, and $\breve{u}_d$ and $\breve{u}_q$ denote the dq-axes voltage references (u_d^*, u_q^*) with the compensation of the delay caused by the digital controller

and the pulsewidth modulation (PWM) of the VSI [24], [32]

$$\begin{bmatrix}\breve{u}_d(k)\\ \breve{u}_q(k)\end{bmatrix}=\begin{bmatrix}\cos\left(1.5\omega(k)T_c\right) & \sin\left(1.5\omega(k)T_c\right)\\ -\sin\left(1.5\omega(k)T_c\right) & \cos\left(1.5\omega(k)T_c\right)\end{bmatrix}\begin{bmatrix}u_d^*(k-1)\\ u_q^*(k-1)\end{bmatrix} \tag{3}$$

where T_c is the controller sampling time. In particular, the terms $D_d V_{\text{dead}}$ and $D_q V_{\text{dead}}$ account for dead-time effects and voltage drops across the power switches and diodes [11]. It is worth highlighting that the motor input voltages are rarely measured in VSI-fed PMSM drives, and commonly the voltage references provided by the dq-axes current regulators are exploited to perform parameter estimation [14], [27]. The motor parameters are the dq-axes stator inductances L_d and L_q, the stator resistance R, and the rotor flux linkage ψ. Note that when $i_d \neq 0$, both D_d and D_q are different from zero and can be computed using phase current and rotor position measurements [24], [33]. Due to the presence of the harmonic content introduced by the distorted coefficients accounting for the PWM of the VSI, an additional equation can be considered [34]

$$\breve{u}_{dhf}(k) = -D_{dhf}(k) V_{\text{dead}} \tag{4}$$

where $\breve{u}_{dhf}$ and D_{dhf} represent the harmonic components of $\breve{u}_d$ and D_d, respectively. Note that five parameters (L_d, L_q, R, ψ, and V_{dead}) appear in equations (1), (2), and (4). As a result, the parameter estimation problem is rank-deficient, and data from at least two distinct steady states of the motor are required to estimate all parameters.

It is well known that motor parameters do not remain constant and change with OCs due to magnetic saturation, temperature, and alternating current (AC) effects. To design the proposed parameter estimation approach, it is necessary to clarify the mathematical relationships between the parameters and the other PMSM variables. The stator inductances are commonly modeled using polynomial functions of the dq-axis currents [27], [35], [36]

$$L_d = L_{d0} + \alpha_{d1} i_d + \alpha_{d2} i_q + \alpha_{d3} i_d^2 + \alpha_{d4} i_d i_q + \alpha_{d5} i_q^2 \tag{5}$$

$$L_q = L_{q0} + \alpha_{q1} i_d + \alpha_{q2} i_q + \alpha_{q3} i_d^2 + \alpha_{q4} i_d i_q + \alpha_{q5} i_q^2. \tag{6}$$

The stator resistance and rotor flux linkage can instead be modeled considering temperature and ac effects as follows [37]:

$$R = R_0\left(1+\alpha(T_s-20^\circ\text{C})\right)\left(1+\frac{\beta\omega^2}{\left(1+\alpha(T_s-20)\right)^{1.5}}\right) \tag{7}$$

$$\psi = \psi_0\left(1+\alpha_{\text{PM}}(T_r-20^\circ\text{C})\right) \tag{8}$$

where T_s and T_r are the stator winding and PM temperatures, α and α_{PM} are the copper and PM temperature coefficients, and β is the frequency coefficient of the ac resistance component. Since the stator winding temperature measurement is usually available in modern PMSM drives, (1) and (2) can be reformulated as follows:

$$\breve{u}_d(k) = R' i_{d\Theta}(k) - L_q \omega(k) i_q(k) - D_d(k) V_{\text{dead}} \tag{9}$$

$$\breve{u}_q(k) = R' i_{q\Theta}(k) + L_d \omega(k) i_d(k) + \psi\omega(k) - D_q(k) V_{\text{dead}} \tag{10}$$

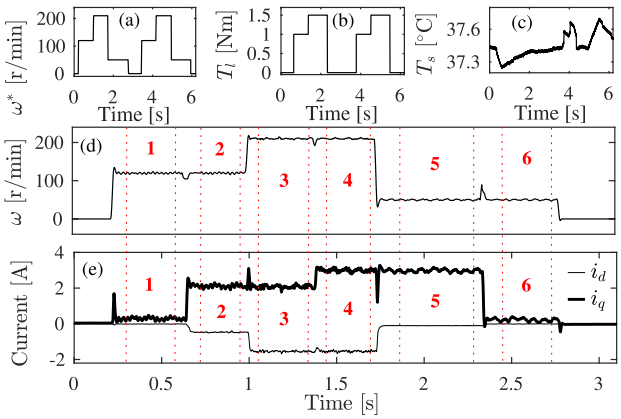

Fig. 1. Example of an operational scenario with a periodic cycle.

with

$$R' = \frac{R}{1+\alpha(T_s-20^\circ\text{C})} \tag{11}$$

$$i_{d\Theta} = i_d\left(1+\alpha(T_s-20^\circ\text{C})\right),\ i_{q\Theta} = i_q\left(1+\alpha(T_s-20^\circ\text{C})\right). \tag{12}$$

III. Proposed Offline Parameter Estimation

Before presenting the proposed offline parameter estimation method, it is important to clarify the constraints and prerequisites that guided its design. These elements were defined to ensure noninvasiveness, flexibility, cost-effectiveness, and ease of large-scale deployment. The constraints considered are as follows.

1) Injection of perturbation signals is not allowed.
2) Execution of dedicated tests is not allowed.
3) Additional equipment and/or sensors are not allowed.
4) Estimation should be feasible even with only two different motor OCs.

The prerequisites are as follows.

1) The PMSM drive is operational and has been precalibrated for the specific application scenario.
2) Measurement data can be acquired from the drive during normal operation.
3) External computing hardware (e.g., dedicated PCs) or cloud-computing platforms are available for storing and processing the measurement data.

It is worth emphasizing that these constraints and prerequisites distinguish the proposed approach from existing offline parameter estimation methods from the very foundation and the earliest stages of its design. In particular, the last constraint is important to guarantee the suitability of the parameter estimation in conditions of data scarcity. Indeed, since the proposed approach relies solely on measurement data acquired during regular on-load motor operation, without any intentional control aimed at performing parameter estimation, the number of available operating points depends exclusively on the specific application scenario. For instance, Fig. 1 illustrates a representative application scenario characterized by a periodic working cycle with only six distinct steady-state operating points. Specifically,

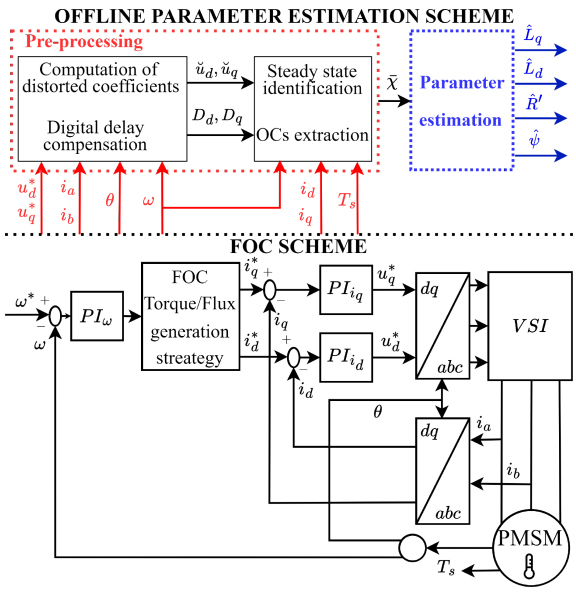

Fig. 2. Overall PMSM control and parameter estimation diagram.

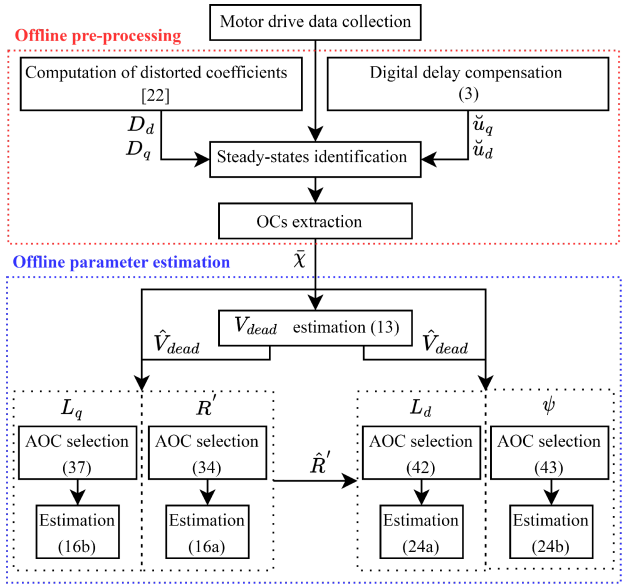

Fig. 3. Flow-chart of the proposed estimation algorithm.

Fig. 1(a) shows the speed reference ω^*, while Fig. 1(b) depicts the corresponding load torque T_l profile. The thermal behavior of the PMSM during the experimental execution of this cycle is presented in Fig. 1(c). Fig. 1(d) and (e) displays the motor speed and the dq-axis currents, respectively, over one period of the working cycle. This example illustrates a typical case of limited data diversity: as highlighted in Fig. 1(d) and (e), the dataset contains only six steady-state operating points at distinct speed/torque combinations.

The overall scheme of the proposed offline parameter estimation is depicted in Fig. 2. A standard field-oriented control (FOC) with proportional–integral (PI) regulators of the PMSM speed and dq-axes currents is considered. The measured motor variables are collected during the regular motor operation without dedicated tests or signal injection and are processed by the proposed offline parameter estimation algorithm (detailed in Fig. 3), which runs on a dedicated PC or a cloud-computing platform. The first task is the collection of the measurement data from the motor drive. In real-world implementations, this operation can be automatically performed exploiting the communication capability of the latest generation drives and edge/cloud computing architectures. In particular, the variables to be collected are the dq-axes voltage references and currents, the electrical rotor speed and position (θ), the phase currents (i_a, i_b) and the stator winding temperature.

The next task involves the preliminary processing of the collected data necessary for parameter estimation. In particular, the dq-axes distorted coefficients are computed as in [24] and the voltage references are corrected according to (3). The R-statistic technique detects the electro-mechanical steady states of the motor, which are periods of constant speed and dq-axes current, as shown in [30]. In this way, the motor transient states are automatically excluded from the dataset.

In the third task, each electro–mechanical steady state is sliced in different time intervals in order to assess the effect of the winding temperature variations. The time intervals are defined ensuring that the stator temperature variation in each of them is less than a given threshold ΔT_s. After the "thermal" slicing of the electro-mechanical steady states, the motor OCs can be extracted and are defined as vectors $\bar{X}_j = \left[\bar{\omega}_j \quad \bar{i}_{dq_j} \quad \bar{\breve{u}}_{dq_j} \quad \bar{D}_{d_j} \quad \bar{D}_{q_j} \quad \bar{T}_{s_j}\right]$, $j = 1, \ldots, N_{OC}$, where the upper bar "$\bar{}$" denotes the average value of the variables in each time interval among the electromechanical steady states. The matrix $\bar{\mathcal{X}} = \{\bar{X}_1, \ldots, \bar{X}_{N_{OC}}\}$ represents the set of all the OCs from the collected data. Note that averaging measurements obtained during electro-mechanical steady states filters out zero-mean noise, improving parameter estimation accuracy [33].

In the next step, the estimation of V_{dead} is performed in all the available OCs in $\bar{\mathcal{X}}$. The estimation of V_{dead} is based on (4). This equation cannot be simply reversed to obtain $\hat{V}_{\text{dead}}$ as $D_{dhf}(k)$ may be zero for some k. Therefore, the proposed approach is to solve the following optimization problem for each extracted OC:

$$\min_{\hat{V}_{\text{dead}_j}} \sum_{k=k_{s_j}}^{k_{e_j}} \left| D_{dhf_j}(k)\hat{V}_{\text{dead}_j} + \breve{u}_{dhf_j}(k) \right| \tag{13}$$

with k_{s_j} and k_{e_j} denoting the initial and final sample of the time interval of the jth OC.

Subsequently, R' and L_q are estimated in all the extracted OCs exploiting the estimations of V_{dead}. Finally, L_d and ψ are estimated in all available OCs using the estimations of V_{dead} and R'. In particular, these last steps involve the selection of the auxiliary operating conditions (AOCs) to overcome the rank-deficiency issue and mitigate estimation errors. In particular, the algorithm designed to estimate L_q, R', L_d, and ψ and supported by the selection procedure of the AOCs is the core of the proposed methodology and the main original contribution of this work. The estimation algorithm is detailed in the following sections.

A. L_q and R' Estimation

The estimation of L_q and R' is affected by the rank-deficiency issue. In particular, to estimate these parameters in an OC, at least another OC is required. In this work, exactly two different OCs will be used to estimate L_q and R. As will be shown later, the availability of more than two OCs is exploited by the proposed algorithm to improve estimation accuracy.

The OC in which a parameter has to be estimated is denoted as main operating condition (MOC), while the OC coupled with the MOC to solve the rank deficiency issue is denoted as AOC. Let us consider (9) written for a generic MOC and AOC by substituting the VSI distorted voltage with its estimation

$$\begin{bmatrix} \bar{\breve{u}}_d^m + \bar{D}_d^m \hat{V}_{\text{dead}}^m \\ \bar{\breve{u}}_q^a + \bar{D}_d^a \hat{V}_{\text{dead}}^a \end{bmatrix} = \begin{bmatrix} \bar{i}_{d\Theta}^m & -\bar{\omega}^m \bar{i}_q^m \\ \bar{i}_{d\Theta}^a & -\bar{\omega}^a \bar{i}_q^a \end{bmatrix} \begin{bmatrix} R' \\ L_q \end{bmatrix} \tag{14}$$

with the superscripts "m" and "a" denoting the variables in the MOC and AOC, respectively. The estimated R' and L_q can be obtained by reversing (14)

$$\begin{bmatrix} \hat{R}' \\ \hat{L}_q \end{bmatrix} = \begin{bmatrix} \bar{i}_{d\Theta}^m & -\bar{\omega}^m \bar{i}_q^m \\ \bar{i}_{d\Theta}^a & -\bar{\omega}^a \bar{i}_q^a \end{bmatrix}^{-1} \begin{bmatrix} \bar{\breve{u}}_d^m + \bar{D}_d^m \hat{V}_{\text{dead}}^m \\ \bar{\breve{u}}_q^a + \bar{D}_d^a \hat{V}_{\text{dead}}^a \end{bmatrix} \tag{15}$$

which leads to the following expressions of the estimations:

$$\hat{R}' = \frac{-\bar{\omega}^a \bar{i}_q^a (\bar{\breve{u}}_d^m + \bar{D}_d^m \hat{V}_{\text{dead}}^m) + \bar{\omega}^m \bar{i}_q^m (\bar{\breve{u}}_q^a + \bar{D}_d^a \hat{V}_{\text{dead}}^a)}{-\bar{\omega}^a \bar{i}_q^a \bar{i}_{d\Theta}^m (1 - r_d)} \tag{16a}$$

$$\hat{L}_q = \frac{-\bar{i}_{d\Theta}^a (\bar{\breve{u}}_d^m + \bar{D}_d^m \hat{V}_{\text{dead}}^m) + \bar{i}_{d\Theta}^m (\bar{\breve{u}}_q^a + \bar{D}_d^a \hat{V}_{\text{dead}}^a)}{-\bar{\omega}^a \bar{i}_q^a \bar{i}_{d\Theta}^m (1 - r_d)} \tag{16b}$$

with

$$r_d = \frac{\bar{\omega}^m \bar{i}_q^m \bar{i}_{d\Theta}^a}{\bar{\omega}^a \bar{i}_q^a \bar{i}_{d\Theta}^m}. \tag{17}$$

Note that it must be $r_d \neq 1$ to obtain a full rank system and correctly estimate the parameters.

The values of the motor parameters are generally different in the MOC and AOC; therefore, estimation errors are inevitable. It is important to analyze these errors to reject estimations affected by low accuracy and to properly select the AOC in case more than two OCs are available. To obtain the expressions of the estimation errors, the following equations derived from (9), including the presence of voltage errors and parameter variations, are considered

$$\bar{\breve{u}}_d^m + \bar{D}_d^m \hat{V}_{\text{dead}} = R'^m \bar{i}_{d\Theta}^m - L_q^m \bar{\omega}^m \bar{i}_q^m + \varepsilon_{u_d}^m \tag{18a}$$

$$\bar{\breve{u}}_d^a + \bar{D}_d^a \hat{V}_{\text{dead}} = R'^a \bar{i}_{d\Theta}^a - L_q^a \bar{\omega}^a \bar{i}_q^a + \varepsilon_{u_d}^a \tag{18b}$$

where R'^m, R'^a, L_q^m, and L_q^a denote the actual values of the parameters in the MOC and AOC, while $\varepsilon_{u_d}^m$ and $\varepsilon_{u_d}^a$ represent voltage errors mainly due to imperfect VSI nonlinearity compensation. By substituting (18) into (16), the following expressions of the estimations are obtained:

$$\hat{R}' = R'^m + \varepsilon_R = R'^m + \varepsilon_{R,\Delta} + \varepsilon_{R,u} \tag{19a}$$

$$\hat{L}_q = L_q^m + \varepsilon_{L_q} = L_q^m + \varepsilon_{L_q,\Delta} + \varepsilon_{L_q,u} \tag{19b}$$

with

$$\varepsilon_{R,\Delta} = \frac{(R'^m - R'^a) r_d}{1 - r_d} - \frac{(L_q^m - L_q^a) \bar{\omega}^m \bar{i}_q^m}{\bar{i}_{d\Theta}^m (1 - r_d)} \tag{20a}$$

$$\varepsilon_{R,u} = \frac{\varepsilon_{u_d}^m - \frac{\bar{\omega}^m \bar{i}_q^m}{\bar{\omega}^a \bar{i}_q^a} \varepsilon_{u_d}^a}{\bar{i}_{d\Theta}^m (1 - r_d)} \tag{20b}$$

and

$$\varepsilon_{L_q,\Delta} = \frac{(R'^m - R'^a) \bar{i}_{d\Theta}^a}{\bar{\omega}^a \bar{i}_q^a (1 - r_d)} - \frac{(L_q^m - L_q^a)}{1 - r_d} \tag{21a}$$

$$\varepsilon_{L_q,u} = \frac{\varepsilon_{u_d}^m \frac{\bar{i}_{d\Theta}^a}{\bar{i}_{d\Theta}^m} - \varepsilon_{u_d}^a}{\bar{\omega}^a \bar{i}_q^a (1 - r_d)}. \tag{21b}$$

Both parameters are influenced by two different types of estimation errors. The first type ($\varepsilon_{R,\Delta}, \varepsilon_{L_q,\Delta}$) arises from parameter variations due to ac and magnetic saturation effects, while the second type ($\varepsilon_{R,u}, \varepsilon_{L_q,u}$) originates from voltage errors caused by imperfect compensation of dead-time effects and voltage drops in the PWM VSI.

B. L_d and ψ Estimation

The estimation of L_d and ψ and the corresponding error analysis is performed with the same logic adopted for L_q and R'. In this case, both the previously estimated V_{dead} and R' are exploited to estimate L_d and ψ.

Let us consider (10) written for the MOC and AOC by substituting the stator resistance and the VSI distorted voltage with their estimations

$$\begin{bmatrix} \bar{\breve{u}}_q^m + \bar{D}_q^m \hat{V}_{\text{dead}}^m - \hat{R}'^m \bar{i}_{q\Theta}^m \\ \bar{\breve{u}}_q^a + \bar{D}_q^a \hat{V}_{\text{dead}}^a - \hat{R}'^a \bar{i}_{q\Theta}^a \end{bmatrix} = \begin{bmatrix} \bar{\omega}^m \bar{i}_d^m & \bar{\omega}^m \\ \bar{\omega}^a \bar{i}_d^a & \bar{\omega}^a \end{bmatrix} \begin{bmatrix} L_d \\ \psi \end{bmatrix}. \tag{22}$$

The estimated d-axis inductance and rotor flux linkage are obtained by reversing (22)

$$\begin{bmatrix} \hat{L}_d \\ \hat{\psi} \end{bmatrix} = \begin{bmatrix} \bar{\omega}^m \bar{i}_d^m & \bar{\omega}^m \\ \bar{\omega}^a \bar{i}_d^a & \bar{\omega}^a \end{bmatrix}^{-1} \begin{bmatrix} \bar{\breve{u}}_q^m + \bar{D}_q^m \hat{V}_{\text{dead}}^m - \hat{R}'^m \bar{i}_{q\Theta}^m \\ \bar{\breve{u}}_q^a + \bar{D}_q^a \hat{V}_{\text{dead}}^a - \hat{R}'^a \bar{i}_{q\Theta}^a \end{bmatrix} \tag{23}$$

which leads to the following expressions of the estimations:

$$\begin{aligned} \hat{L}_d = {} & \frac{\bar{\omega}^a (\bar{\breve{u}}_q^m + \bar{D}_q^m \hat{V}_{\text{dead}}^m - \hat{R}'^m \bar{i}_{q\Theta}^m)}{\bar{\omega}^a \bar{\omega}^m \bar{i}_d^m (1 - r_q)} \\ & - \frac{\bar{\omega}^m (\bar{\breve{u}}_q^a + \bar{D}_q^a \hat{V}_{\text{dead}}^a - \hat{R}'^m \bar{i}_{q\Theta}^m)}{\bar{\omega}^a \bar{\omega}^m \bar{i}_d^m (1 - r_q)} \end{aligned} \tag{24a}$$

$$\begin{aligned} \hat{\psi} = {} & \frac{-\bar{\omega}^a \bar{i}_d^a (\bar{\breve{u}}_q^m + \bar{D}_q^m \hat{V}_{\text{dead}}^m - \hat{R}'^m \bar{i}_{q\Theta}^m)}{\bar{\omega}^a \bar{\omega}^m \bar{i}_d^m (1 - r_q)} \\ & + \frac{\bar{\omega}^m \bar{i}_d^m (\bar{\breve{u}}_q^a + \bar{D}_q^a \hat{V}_{\text{dead}}^a - \hat{R}'^m \bar{i}_{q\Theta}^m)}{\bar{\omega}^a \bar{\omega}^m \bar{i}_d^m (1 - r_q)} \end{aligned} \tag{24b}$$

with

$$r_q = \frac{\bar{i}_d^a}{\bar{i}_d^m}. \tag{25}$$

In this case it must be $r_q \neq 1$ to obtain a system with rank two and correctly estimate the parameters.

To obtain the expressions of the estimation errors, the following equations derived from (10) including the presence of voltage errors and parameter variations are considered:

$$\breve{u}_q^m + \bar{D}_q^m \hat{V}_{\text{dead}} = R'^m \bar{i}_{q\Theta}^m + L_d^m \bar{\omega}^m \bar{i}_d^m + \bar{\omega}^m \psi^m + \varepsilon_{u_q}^m \quad (26a)$$

$$\breve{u}_q^a + \bar{D}_q^a \hat{V}_{\text{dead}} = R'^a \bar{i}_{q\Theta}^a + L_d^a \bar{\omega}^a \bar{i}_d^a + \bar{\omega}^a \psi^a + \varepsilon_{u_q}^a \quad (26b)$$

where $\varepsilon_{u_q}^m$ and $\varepsilon_{u_q}^a$ represent the q-axis voltage errors. By substituing (26) into (24), the following expression of the estimations are obtained:

$$\hat{L}_d = L_d^m + \varepsilon_{L_d} = L_d^m + \varepsilon_{L_d,\Delta} + \varepsilon_{L_d,\hat{R}} + \varepsilon_{L_d,u} \quad (27a)$$

$$\hat{\psi} = \psi + \varepsilon_\psi = \psi^m + \varepsilon_{\psi,\Delta} + \varepsilon_{\psi,\hat{R}} + \varepsilon_{\psi,u} \quad (27b)$$

with

$$\varepsilon_{L_d,\Delta} = \frac{(L_d^m - L_d^a) r_q}{(1 - r_q)} - \frac{\psi^m - \psi^a}{i_d^m (1 - r_q)} \quad (28a)$$

$$\varepsilon_{L_d,\hat{R}} = \frac{\varepsilon_R^m \bar{i}_{q\Theta}^m - \varepsilon_R^a \frac{\bar{i}_{q\Theta}^a \omega^m}{\omega^a}}{\bar{\omega}^m \bar{i}_d^m (1 - r_q)} \quad (28b)$$

$$\varepsilon_{L_d,u} = \frac{\varepsilon_{u_q}^m - \varepsilon_{u_q}^a \frac{\omega^m}{\omega^a}}{\bar{\omega}^m \bar{i}_d^m (1 - r_q)} \quad (28c)$$

and

$$\varepsilon_{\psi,\Delta} = \frac{(\psi^a - \psi^m)}{1 - r_q} + \frac{\bar{i}_d^a (L_d^a - L_d^m)}{(1 - r_q)} \quad (29a)$$

$$\varepsilon_{\psi,\hat{R}} = \frac{\varepsilon_R^a \bar{i}_{q\Theta}^a - \varepsilon_R^m \frac{\bar{i}_{q\Theta}^m \bar{i}_d^a \omega^a}{\bar{i}_d^m \omega^m}}{\omega^a (1 - r_q)} \quad (29b)$$

$$\varepsilon_{\psi,u} = \frac{\varepsilon_{u_q}^a - \varepsilon_{u_q}^m \frac{\bar{i}_d^a \omega^a}{\bar{i}_d^m \omega^m}}{\omega^a (1 - r_q)} \quad (29c)$$

where $\varepsilon_R^m = R'^m - \hat{R}'^m$ and $\varepsilon_R^a = R'^a - \hat{R}'^a$ are the stator resistance estimation errors in the MOC and AOC. It is worth noticing that, in this case, with respect to the estimation of R' and L_q, an additional error component related the stator resistance estimation error is present.

IV. AOC Selection

The previous section demonstrates that the accuracy of estimated parameters is affected by voltage errors caused by an imperfect compensation of the VSI nonlinearity and by parameter variations caused by temperature, AC and magnetic saturation effects. Additionally, the theoretical formulas show that the estimation errors are largely dependent on the choice of the AOC. As a consequence, it is of paramount importance to determine, for each parameter, the set of the AOCs that mitigate the estimation errors. To do so, this section first presents how the estimation errors are calculated and the AOCs are selected (Section IV-A) and then outlines the rational behind the choice of the hyperparameters required by the proposed approach (Section IV-B).

A. AOC Selection Procedure

Given the vector of the available OCs $V_{\text{OC}} = [1, 2, \ldots, N_{\text{OC}}]$ and considering for instance the estimation of R', the problem is to determine the vector

$$V_R^{\text{AOC}} = [\text{AOC}_{R,1}, \text{AOC}_{R,2}, \ldots, \text{AOC}_{R,N_{\text{OC}}}] \quad (30)$$

with $\text{AOC}_{R,j} \in V_{\text{OC}}$, such that $\text{AOC}_{R,j}$ is the AOC used to estimate R' in the jth OC mitigating the estimation errors. The same problem must be solved for the estimation of the other parameters in order to determine the vectors of the AOCs $V_{L_d}^{\text{AOC}}$, $V_{L_q}^{\text{AOC}}$ and V_ψ^{AOC}.

Let's first focus on the selection of the AOCs for the estimation of R'. The exact computation of the estimation errors is obviously not possible given the inability to predict in advance the measurement errors and parameter variations. Hence, the proposed strategy is based on the minimization of an error function $\tilde{\varepsilon}_R$ designed to act as a majorant of the actual error ε_R. This error function is computed on the basis of previous information and assumptions on the motor drive

$$\tilde{\varepsilon}_R = \tilde{\varepsilon}_{R,\Delta} + \tilde{\varepsilon}_{R,u} > \varepsilon_{R,\Delta} + \varepsilon_{R,u} \quad (31)$$

with

$$\tilde{\varepsilon}_{R,\Delta} = \left| \frac{(\tilde{R}'^m - \tilde{R}'^a) r_d}{1 - r_d} \right| + \left| \frac{(\tilde{L}_q^m - \tilde{L}_q^a) \bar{\omega}^m \bar{i}_q^m}{\bar{i}_{d\Theta}^m (1 - r_d)} \right| \quad (32a)$$

$$\tilde{\varepsilon}_{R,u} = \left| \frac{\left|\tilde{\varepsilon}_{u_d}^m\right| + \left| \frac{\bar{\omega}^m \bar{i}_q^m}{\bar{\omega}^a \bar{i}_q^a} \tilde{\varepsilon}_{u_d}^a \right|}{\bar{i}_{d\Theta}^m (1 - r_d)} \right| \quad (32b)$$

where $\tilde{R}'^m$, $\tilde{R}'^a$, $\tilde{L}_q^m$, and $\tilde{L}_q^a$ are the supposed values of R' and L_d in the MOC and AOC, while $\tilde{\varepsilon}_{u_d}^m$ and $\tilde{\varepsilon}_{u_d}^a$ are the supposed d-axis voltage errors, whose choice is discussed below. The AOC for the jth MOC is then selected by minimizing $\tilde{\varepsilon}_R$ according to this constrained optimization

$$\text{AOC}_{R,j} = \underset{i=1,\ldots,N_{\text{OC}}}{\text{argmin}} \ \tilde{\varepsilon}_{R_{j,i}}$$

$$\text{s.t.} \quad r_d < r_{\max} \text{ or } r_d > r_{\min}, \quad \text{and} \quad \tilde{\varepsilon}_R < p \cdot \tilde{R}'^j. \quad (33)$$

where $\tilde{\varepsilon}_{R_{j,i}} = \tilde{\varepsilon}_R$ having chosen the jth OC as MOC and the ith OC as AOC, $r_{\max} < 1$ and $r_{\min} > 1$ are two tunable thresholds which avoid choosing r_d close to 1, while p is the rejection threshold, arbitrarily tunable between 0 and 1. Note that the $argmin$ operator denotes the discrete search over a vector of N_{OC} available OCs of the AOC that minimizes the error function. In other words, by selecting the AOC that minimizes $\tilde{\varepsilon}_R$, it is more likely to obtain a low actual estimation error ε_R. Note that the estimation is not performed (rejected estimation) if does not exist an AOC satisfying the conditions in (33).

The same approach is adopted for the estimation of L_q by computing the majorant of ε_{L_q}

$$\tilde{\varepsilon}_{L_q} = \tilde{\varepsilon}_{L_q,\Delta} + \tilde{\varepsilon}_{L_q,u} > \varepsilon_{L_q,\Delta} + \varepsilon_{L_q,u} \quad (34)$$

with

$$\tilde{\varepsilon}_{L_q,\Delta} = \left| \frac{(\tilde{R}'^m - \tilde{R}'^a) \bar{i}_{d\Theta}^a}{\bar{\omega}^a \bar{i}_q^a (1 - r_d)} \right| + \left| \frac{(\tilde{L}_q^m - \tilde{L}_q^a)}{1 - r_d} \right| \quad (35a)$$

$$\tilde{\varepsilon}_{L_q,u} = \left| \frac{\left|\tilde{\varepsilon}^m_{u_d} \frac{\bar{i}^a_{d\Theta}}{\bar{i}^m_{d\Theta}}\right| + \left|\tilde{\varepsilon}^a_{u_d}\right|}{\bar{\omega}^a \bar{i}^a_q (1-r_d)} \right|. \tag{35b}$$

With the same logic, the AOC is selected by minimizing $\tilde{\varepsilon}_{L_q}$ for each available OC

$$\begin{aligned} \text{AOC}_{L_q,j} = & \underset{i=1,\ldots,N_{\text{OC}}}{\text{argmin}} \ \tilde{\varepsilon}_{L_{qj,i}} \\ & \text{s.t.} \ \ r_d < r_{\min} \text{ or } r_d > r_{\max}, \ \text{ and } \ \tilde{\varepsilon}_{L_q} < p \cdot \tilde{L}^j_q. \end{aligned} \tag{36}$$

Similarly, the majorants of $\tilde{\varepsilon}_{L_d}$ and $\tilde{\varepsilon}_{\psi}$ are defined as

$$\tilde{\varepsilon}_{L_d} = \tilde{\varepsilon}_{L_d,\Delta} + \tilde{\varepsilon}_{L_d,\hat{R}} + \tilde{\varepsilon}_{L_d,u} > \varepsilon_{L_d,\Delta} + \varepsilon_{L_d,\hat{R}} + \varepsilon_{L_d,u} \tag{37}$$

$$\tilde{\varepsilon}_{\psi} = \tilde{\varepsilon}_{\psi,\Delta} + \tilde{\varepsilon}_{\psi,\hat{R}} + \tilde{\varepsilon}_{\psi,u} > \varepsilon_{\psi,\Delta} + \varepsilon_{\psi,\hat{R}} + \varepsilon_{\psi,u} \tag{38}$$

with

$$\tilde{\varepsilon}_{L_d,\Delta} = \left| \frac{(\tilde{L}^m_d - \tilde{L}^a_d) r_q}{(1-r_q)} \right| + \left| \frac{\tilde{\psi}^m - \tilde{\psi}^a}{i^m_d (1-r_q)} \right| \tag{39a}$$

$$\tilde{\varepsilon}_{L_d,\hat{R}} = \left| \frac{\left|\tilde{\epsilon}_R \bar{i}^m_{q\Theta}\right| + \left|\tilde{\epsilon}_R \frac{\bar{i}^a_{q\Theta}\omega^m}{\omega^a}\right|}{\bar{\omega}^m \bar{i}^m_d (1-r_q)} \right| \tag{39b}$$

$$\tilde{\varepsilon}_{L_d,u} = \left| \frac{\left|\tilde{\varepsilon}^m_{u_q}\right| + \left|\tilde{\varepsilon}^a_{u_q} \frac{\omega^m}{\omega^a}\right|}{\bar{\omega}^m \bar{i}^m_d (1-r_q)} \right| \tag{39c}$$

and

$$\tilde{\varepsilon}_{\psi,\Delta} = \left| \frac{(\tilde{\psi}^a - \tilde{\psi}^m)}{1-r_q} \right| + \left| \frac{\bar{i}^a_d (\tilde{L}^a_d - \tilde{L}^m_d)}{(1-r_q)} \right| \tag{40a}$$

$$\tilde{\varepsilon}_{\psi,\hat{R}} = \left| \frac{\left|\tilde{\epsilon}_R \bar{i}^a_{q\Theta}\right| + \left|\tilde{\epsilon}_R \frac{\bar{i}^m_{q\Theta}\bar{i}^a_d\omega^a}{\bar{i}^m_d\omega^m}\right|}{\omega^a (1-r_q)} \right| \tag{40b}$$

$$\tilde{\varepsilon}_{\psi,u} = \left| \frac{\left|\tilde{\varepsilon}^a_{u_q}\right| + \left|\varepsilon^m_{u_q} \frac{\bar{i}^a_d\omega^a}{\bar{i}^m_d\omega^m}\right|}{\omega^a (1-r_q)} \right| \tag{40c}$$

where $\tilde{\epsilon}_R$ is the supposed stator resistance estimation error, $\tilde{\varepsilon}_{u_q}$ is the supposed q-axis voltage error and $\tilde{L}^m_d$, $\tilde{L}^a_d$, $\tilde{\psi}^m$, and $\tilde{\psi}^a$ are the supposed values of L_d and ψ in the MOC and AOC. Likewise, the AOCs for L_d and ψ are selected by minimizing $\tilde{\varepsilon}_{L_d}$ and $\tilde{\varepsilon}_{\psi}$

$$\begin{aligned} \text{AOC}_{L_d,j} = & \underset{i=1,\ldots,N_{\text{OC}}}{\text{argmin}} \ \tilde{\varepsilon}_{L_{dj,i}} \\ & \text{s.t.} \ \ r_q < r_{\min} \text{ or } r_q > r_{\max}, \ \text{ and } \ \tilde{\varepsilon}_{L_d} < p \cdot \tilde{L}^j_d. \end{aligned} \tag{41}$$

$$\begin{aligned} \text{AOC}_{\psi,j} = & \underset{i=1,\ldots,N_{\text{OC}}}{\text{argmin}} \ \tilde{\varepsilon}_{\psi_{j,i}} \\ & \text{s.t.} \ \ r_q < r_{\min} \text{ or } r_q > r_{\max}, \ \text{ and } \ \tilde{\varepsilon}_{\psi} < p \cdot \tilde{\psi}^j. \end{aligned} \tag{42}$$

It is worth remarking that minimizing the error functions ($\tilde{\varepsilon}_{L_d}$, $\tilde{\varepsilon}_{L_q}, \tilde{\varepsilon}_R, \tilde{\varepsilon}_{\psi}$) does not guarantee the selection of the best possible AOCs. However, the minimization of these functions allows mitigating the actual estimation errors and avoid the selection of the worst OCs.

B. Hyperparameters Selection

The computation of the error functions requires some a-priori assumptions on the parameters, on the voltage errors ($\varepsilon_{u_d}, \varepsilon_{u_q}$) and on the stator resistance estimation errors (ϵ_R).

For example, the calculation of $\tilde{\varepsilon}_R$ requires the supposed values $\tilde{R}'^x$ and $\tilde{L}^x_q$ ($x = m, a$) which can be determined with the following formulas derived from (7) and (6):

$$\tilde{R}'^x = \tilde{R}_0 \left(1 + \frac{\tilde{\beta}\omega^{x2}}{(1 + \alpha(T^x_s - 20))^{1.5}} \right) \tag{43}$$

$$\tilde{L}^x_q = \tilde{L}_{q0} + \tilde{\alpha}_{q1} i^x_d + \tilde{\alpha}_{q2} i^x_q + \tilde{\alpha}_{q3} i^{x2}_d + \tilde{\alpha}_{q4} i^x_d i^x_q + \tilde{\alpha}_{q5} i^{x2}_q \tag{44}$$

where $\tilde{L}_{q0}, \tilde{\alpha}_{q1}, \ldots, \tilde{\alpha}_{q5}$, $\tilde{R}_0$, and $\tilde{\beta}$ are supposed coefficients. In a similar manner, the supposed value of L_d can be calculated with a formula similar to (44) while for ψ the following equation can be used:

$$\tilde{\psi}^x = \tilde{\psi}_0 \left(1 + \tilde{\alpha}_{\text{PM}} (T^x_s - 20)\right). \tag{45}$$

where $\tilde{\psi}_0$ is the supposed value of ψ at 20 °C while $\tilde{\alpha}_{\text{PM}}$ is the supposed PM temperature coefficient. Note that (45) is derived from (8) assuming $T_r = T_s$ since the rotor temperature measurement is usually not available.

Stating the obvious, there are several parameters to assume in order to calculate the supposed parameters with (43), (44), and (45). Regarding $\tilde{L}_{q0}$ in (44), the nominal value from the motor datasheet can be used, whereas the coefficients $\tilde{\alpha}_{q1}, \ldots, \tilde{\alpha}_{q5}$ can be obtained assuming the values of $\tilde{L}_q(i_d, i_q)$ in five different dq-axes current conditions. The same approach can be also adopted for $\tilde{L}_d$. Concerning the assumptions of the coefficients required for the resistance $\tilde{R}'$ calculation in (44), $\tilde{R}_0$ can be set equal to the datasheet value while $\tilde{\beta}$ can be selected according to

$$\beta \omega^2_n = y_\beta \tag{46}$$

where ω_n is the rated electrical speed and y_β has to be chosen. In absence of relevant information on the motor it is suggested to assign a value in the range [0 1]. Indeed, assuming $y_\beta = 1$ corresponds to having an ac stator resistance at ω_n twice the dc value, which is a reasonable assumption (unless dealing with high speed/frequency motors [38]). Regarding $\tilde{\psi}$, $\tilde{\psi}_0$ can be set equal to the nominal value while $\tilde{\alpha}_{\text{PM}}$ can be chosen in the range $[-0.2 \ -0.05]$ %/°C, which are typical values for rare earth magnets.

The dq-axes voltage errors can be calculated according to the following formulas:

$$\varepsilon^x_{u_q} = \bar{D}^x_q \Delta V_{\text{dead}} \tag{47a}$$

$$\varepsilon^x_{u_d} = \bar{D}^x_d \Delta V_{\text{dead}} \tag{47b}$$

where ΔV_{dead} is a tuning parameter, which expresses the supposed absolute estimation error of the VSI distorted voltage. The approximate value of V_{dead} can be determined using datasheet information on the VSI, as shown in [11]. Considering that V_{dead}

TABLE I
HYPERPARAMETERS OF THE PROPOSED ALGORITHM

Parameter	Value or range
L_{d0}, L_{q0}, ψ_{m0}, R_0	Datasheet value
p	[0 0.5]
r_{min}, r_{max}	< 1, > 1
y_β	[0 1]
$\tilde{\alpha}_{PM}$	[−0.2 −0.05]
ΔV_{dead}	[0 0.5]

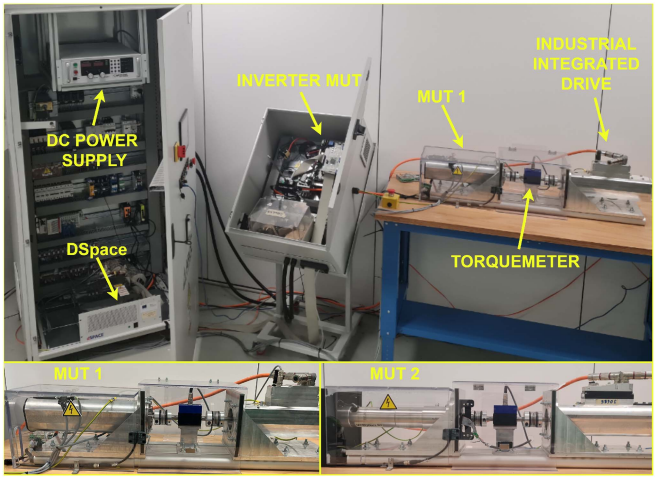

Fig. 4. Experimental set-up layout.

TABLE II
PARAMETERS OF THE TWO TESTED MOTORS

Parameter	Unit	MUT 1	MUT 2
Rated power	kW	0.14	0.25
Rated torque	Nm	2.65	2.4
Rated speed	r/min	500	1000
Rated current	A	1.2	4.0
Number of pole pairs	–	5	7
R_0	Ω	22.09	1.97
ψ_{m0}	Wb	0.295	0.0573
L_{d0}	H	0.0767	0.0091
L_{q0}	H	0.0964	0.0122
β	$1/(rad/s)^2$	$1.84 \cdot 10^{-6}$	$0.25 \cdot 10^{-6}$

TABLE III
SELECTED HYPERPARAMETERS

Parameter	Case 1	Case 2	Case 3
p	0.25	0.25	0.25
r_{min}	0.75	0.75	0.75
r_{max}	1.25	1.25	1.25
$\tilde{R}_0$	1.04 R_0	0.95 R_0	0.84 R_0
$\tilde{\psi}_0$	0.97 ψ_0	1.03 ψ_0	0.88 ψ_0
$\tilde{L}_{d0}$	1.02 L_{d0}	1.34 L_{d0}	0.93 L_{d0}
$\tilde{L}_{q0}$	0.97 L_{q0}	0.94 L_{q0}	1.16 L_{q0}
$\tilde{\alpha}_{PM}$	−0.1 %/°C	−0.15 %/°C	−0.2 %/°C
$\tilde{\beta}$	1.13β	0.56β	2.1β
ΔV_{dead}	0.17 V	0.41 V	0.07 V

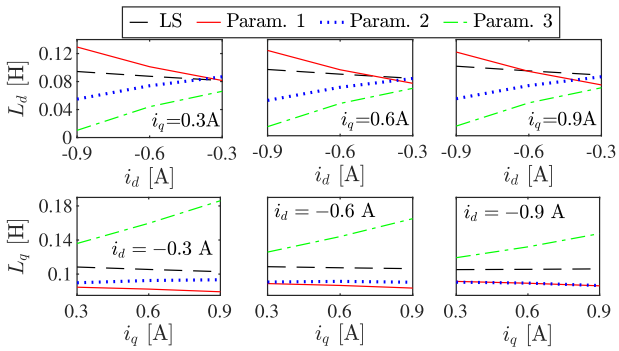

Fig. 5. Actual and supposed inductances of MUT1.

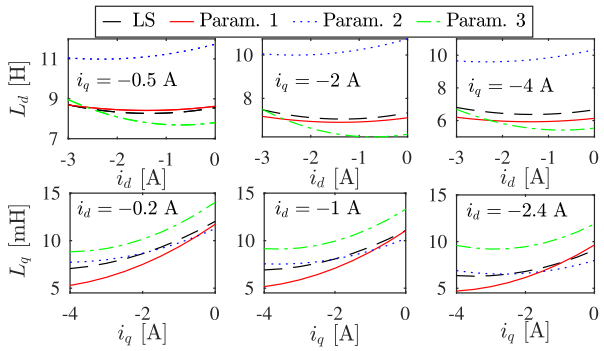

Fig. 6. Actual and supposed inductances of MUT2.

rarely overcomes 2V in standard drives [39], ΔV_{dead} has been prudently set in the range [0 0.5] V.

Finally, concerning the stator resistance estimation error, it can be set $\epsilon_R = \tilde{\varepsilon}_R/4$ if an estimation of R' is available. Otherwise, it is set $\tilde{R}' = \tilde{R}_0$ into (24) and $\epsilon_R = p\tilde{R}_0/4$. Table I summarizes the main hyperparameters of the proposed approach that must be preselected a-priori.

V. EXPERIMENTAL ASSESSMENT

The proposed parameter estimation technique has been validated on two experimental datasets obtained by testing two PMSMs on an instrumented test rig, shown in Fig. 4. The motors under test (MUTs) details are listed in Table II. The MUTs are controlled via the dSPACE plaform (DS1006/FPGA5203) and fed by a custom designed IGBT-based VSI while the stator winding temperature is measured using a PT1000. During test campaign, the MUTs are driven by a speed-controlled industrial drive, while their dq-axes currents were controlled using a standard FOC using PI regulators. The validation is carried out considering three different hyperparametrizations of the algorithm designed for the selection of the AOCs, which are summarized in Table III. Note that this table applies to both MUTs. It should be noted that inaccuracies have been purposely added in the supposed parameter values in order to make the parameter estimation more realistic and assess its robustness. Figs. 5 and 6 show the actual and supposed trends of the dq-axes inductances with the stator currents for the MUT1 and MUT2, respectively. As can be seen, the supposed trends in inductances deviate significantly from the actual ones, making the parameter estimation even more challenging.

The actual parameters reported in Table II and the L_d and L_q trends in Figs. 5 and 6 have been obtained through the

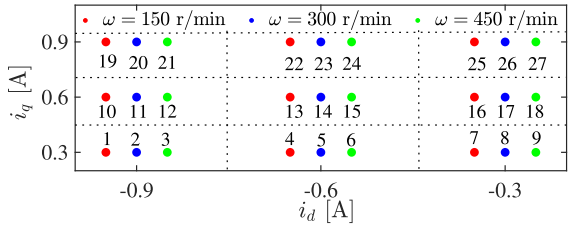

Fig. 7. Experimental dataset for parameter estimation (MUT1).

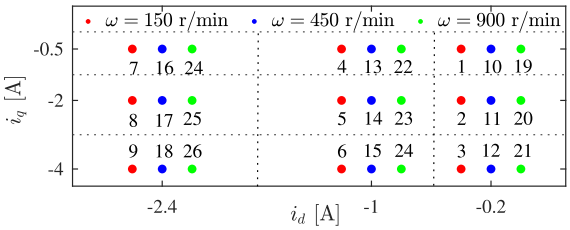

Fig. 8. Experimental dataset for parameter estimation (MUT2).

decoupled least squares (LS) method presented in [27]. This method considers parameter variation functions (including ac effects and magnetic saturation effects) and inverter nonlinearity, providing accurate estimations in presence of large experimental datasets. In particular, the model adopted to apply the decoupled LS method is the following one:

$$\bar{\breve{u}}_d = x_1 - \bar{\omega} y_1, \quad \bar{\breve{u}}_q = x_2 + \bar{\omega} y_2 \tag{48}$$

with

$$\begin{cases} x_1 &= R_0 \bar{i}_{d\Theta} + k_R \frac{\bar{\omega}^2 \bar{i}_{d\Theta}}{(1+\alpha(\bar{T}_s - 20))^{1.5}} + \bar{D}_d V_{\text{dead}} \\ x_2 &= R_0 \bar{i}_{q\Theta} + k_R \frac{\bar{\omega}^2 \bar{i}_{q\Theta}}{(1+\alpha(\bar{T}_s - 20))^{1.5}} + \bar{D}_q V_{\text{dead}} \\ y_1 &= (L_{q0} + \alpha_{q1} \bar{i}_d + \alpha_{q2} \bar{i}_q \\ &\quad + \alpha_{q3} \bar{i}_d^2 + \alpha_{q4} \bar{i}_d \bar{i}_q + \alpha_{q5} \bar{i}_q^2) \bar{i}_q \\ y_2 &= (L_{d0} + \alpha_{d1} \bar{i}_d + \alpha_{d2} \bar{i}_q \\ &\quad + \alpha_{d3} \bar{i}_d^2 + \alpha_{d4} \bar{i}_d \bar{i}_q + \alpha_{d5} \bar{i}_q^2) \bar{i}_d + \psi_0 \end{cases}, \tag{49}$$

in which $k_R = \beta R_0$. According to this method, x_1, x_2, y_1, and y_2 are first estimated from (48) written for all available OCs. Then, x_1 and x_2 are used to estimate R_0, k_R, and V_{dead} and y_1 and y_2 are used to estimate L_{d0}, L_{q0}, $\alpha_{d1}, \ldots, \alpha_{d5}$, $\alpha_{q1}, \ldots, \alpha_{q5}$, and ψ_0 according to (49). Finally, these estimated coefficients are used to compute the values of the motor parameters in each OC in the dataset according to the following formulas:

$$\begin{aligned} L_{d_j} &= L_{d0} + \alpha_{d1} \bar{i}_{d_j} + \alpha_{d2} \bar{i}_{q_j} + \alpha_{d3} \bar{i}_{d_j}^2 + \alpha_{d4} \bar{i}_{d_j} \bar{i}_{q_j} + \alpha_{d5} \bar{i}_{q_j}^2 \\ R'_j &= R_0 + k_R \frac{\bar{\omega}_j^2 \bar{i}_{d\Theta_j}}{(1+\alpha(\bar{T}_{s_j} - 20))^{1.5}} \\ \psi_j &= \psi_0, \\ L_{q_j} &= L_{q0} + \alpha_{q1} \bar{i}_{d_j} + \alpha_{q2} \bar{i}_{q_j} + \alpha_{q3} \bar{i}_{d_j}^2 + \alpha_{q4} \bar{i}_{d_j} \bar{i}_{q_j} + \alpha_{q5} \bar{i}_{q_j}^2. \end{aligned} \tag{50}$$

The decoupled LS method has been applied to two datasets comprising 48 and 75 OCs for MUT1 and MUT2, respectively. The resulting estimations are used as reference values to assess the accuracy of the proposed approach, as well as other existing estimation methods from the literature, in the following sections.

A. Analysis With the Full Dataset

The proposed technique has been validated on two distinct experimental dataset consisting of 27 OCs featuring different speeds and dq-axes currents; all of them are depicted and numbered in Figs. 7 and 8 for MUT1 and MUT2, respectively. In particular, the first dataset is a subset of the dataset used to obtain the reference values of the motor parameters through the decoupled LS method. Fig. 9 shows the measurements collected during the OCs 1 and 24 of the first dataset.

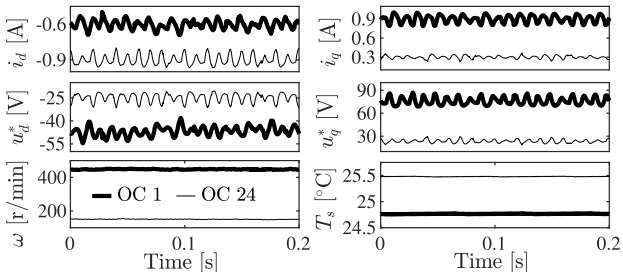

Fig. 9. Measurements collected during OCs 1 and 24 of MUT1.

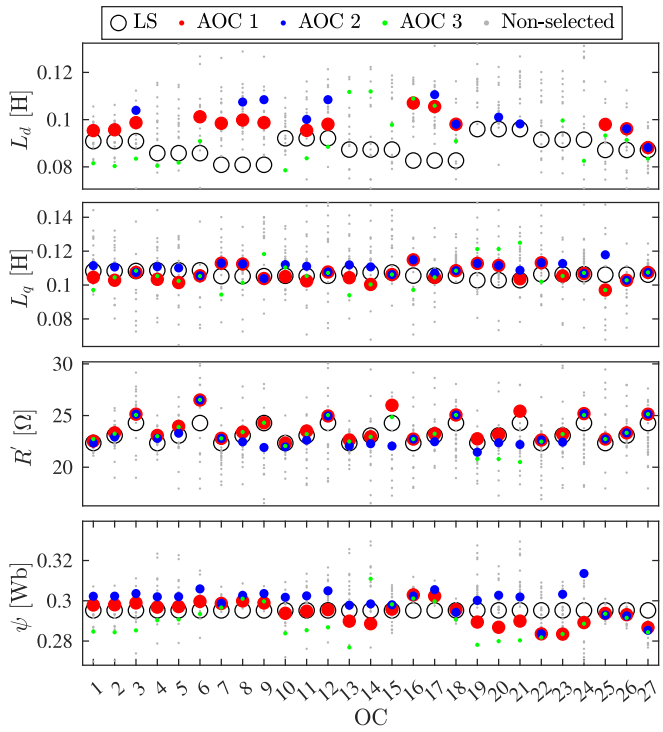

Fig. 10. Parameter estimations obtained by the proposed method assuming the availability of the full dataset of MUT1.

The aim of the first analysis is to assess the capability of the proposed algorithm in selecting AOCs that mitigate estimation errors; therefore, this analysis is performed assuming the availability of the entire datasets in Figs. 7 and 8. Figs. 10 and 11

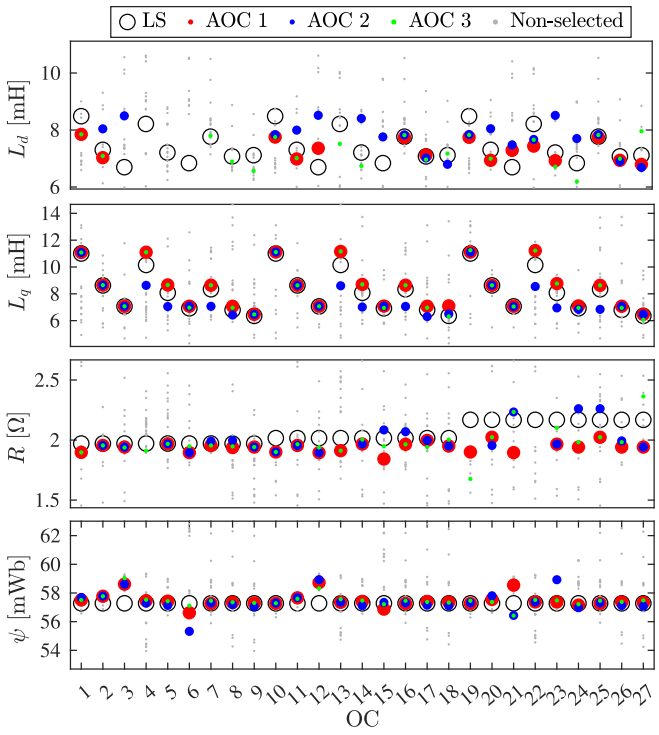

Fig. 11. Parameter estimations obtained by the proposed method assuming the availability of the full dataset of MUT2.

TABLE IV
MAPEs [%] Obtained With the Full Datasets Under Different Hyperparametrizations

Parameter	MUT 1 *Hyperparametrizations*			MUT 2 *Hyperparametrizations*		
	First	Second	Third	First	Second	Third
L_d	14.25	16.28	15.10	5.20	10.19	5.03
L_q	3.97	4.24	6.17	3.78	6.17	3.12
R'	2.36	3.28	3.05	5.23	3.94	4.25
ψ	1.51	2.36	2.90	0.51	0.73	0.50

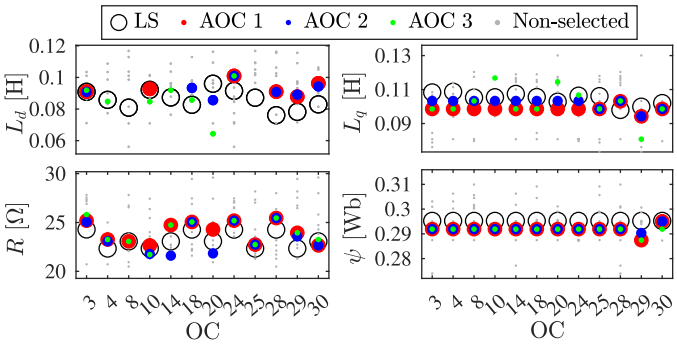

Fig. 12. Parameter estimations obtained by the proposed method on the MUT1 assuming the availability of a reduced dataset including OCs with $i_d = 0$.

illustrate the results for the two MUTs. For each OC (acting as MOC), the figures show the estimations obtained with the AOCs selected according to the three different hyperparametrizations in Table III (red, blue, and green dots). The computational time required to estimate all parameters for each OC in the dataset, using a MATLAB PC equipped with an Intel Xeon E5-1620 v2 @ 3.50 GHz processor and 16 GB of RAM, is approximately 5.1 ms. This computational time also includes the AOC selection procedure. The grey dots instead represent the estimations obtained when using as AOCs other available OCs not selected by the proposed algorithm. The black circles represent the reference values obtained with the decoupled LS. The large dispersion of the grey dots in both figures indicates that the estimation accuracy is highly sensitive to the used AOCs, emphasizing the importance of carefully selecting the AOCs.

As can be observed, despite the significant differences in the three hyperparameter settings, the proposed method selects the same AOCs or AOCs that result in equivalent estimation accuracy in most circumstances, particularly when considering the estimation of L_q, R', and ψ. When it comes to estimating L_d, the selected AOCs are instead more dispersed and higher estimation errors are obtained. This occurs because, due to excessively high values of the error functions, the proposed algorithm was unable to find suitable AOCs satisfying (41) for all investigated MOCs. This is the reason why the red, blue and green dots are not shown for some OCs. On the contrary, for the other parameters, the proposed approach always found acceptable AOCs. Although L_d and L_q have similar nominal values, the higher estimation errors observed for L_d can be attributed to two main factors. First, as shown in (21) and (28), unlike L_q, the estimation of L_d is influenced by errors in R'. Second, the coefficients r_d and r_q, which appear in these equations and depend on the chosen AOCs, exhibit different behaviors across the dataset. Specifically, according to (17) and (25), the coefficient r_d (which affects the estimation of L_q) depends on multiple variables and therefore spans a wider range of values. This variability allows for the selection of AOCs that better mitigate estimation errors. For example, for MUT1, when OC 21 is used as the MOC, the ranges for r_d and r_q are $[0.33, 9]$ and $[0.33, 1]$, respectively.

The figures also clearly illustrate that, for L_q, R', and ψ, in the majority of cases, the selected AOCs are among the best available, proving the effectiveness of the proposed strategy. However, under certain specific OCs, varying hyperparameter settings may sometimes result in the choice of subpar OCs. This is evident for instance, for MUT1, considering the estimations of ψ in OCs 1, 2, and 3 and 23 obtained with the third set of hyperparameters; in OCs 22 and 23 with the first hyperparametrization; and in OC 24 with the second hyperparametrization. The mean absolute percentage errors (MAPEs) obtained with the three hyperparametrizations for the two MUTs are summarized in Table IV. These results show that the proposed approach is not highly sensitive to the hyperparameter configurations. In addition, the results highlight a consistent behavior of the estimation algorithm on both datasets.

B. Analysis With a Reduced Dataset Including OCs With $i_d = 0$

To evaluate the performance of the proposed approach in scenarios including OCs, where $i_d = 0$, Fig. 12 presents the results obtained using a different dataset for the MUT1. This

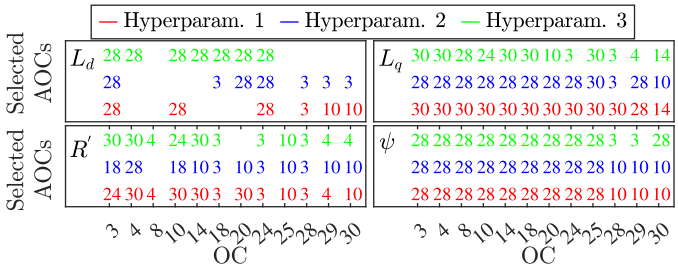

Fig. 13. AOCs selected by the proposed method assuming the availability of a reduced dataset including OCs with $i_d = 0$.

dataset comprises only 12 OCs: the first nine (3, 4, 8, 10, 14, 18. 20, 24, 25) are taken from the dataset shown in Fig. 7, while the last three (28, 29, 30) correspond to OCs with $i_d = 0$. These three OCs have speeds of 400, 150, 300 r/min, and q -axis currents of 0.3, 0.6, 0.9A, respectively. As it can be seen, the results obtained on the three OCs with $i_d = 0$ exhibit similar accuracy compared to the ones obtained on the OCs with $i_d \neq 0$. It is also insightful to analyze the AOCs selected by the proposed method on this dataset, as illustrated in Fig. 13. This figure reports, for each OC in the dataset, the AOCs selected under the three hyperparameter configurations. As can be observed, OCs with $i_d = 0$ are frequently chosen as optimal AOCs to support the estimation in OCs where $i_d \neq 0$. These results demonstrate the ability of the proposed algorithm to effectively operate in scenarios that include OCs with $i_d = 0$.

C. Comparison With Online Noninvasive Approaches

In this section, the proposed method is compared on the MUT1 dataset to two online noninvasive approaches. The first one is the FP method. This approach tackles the rank deficiency issue by setting some parameters to their nominal values and thereby reducing the number of the parameters to be estimated [39]. In this way, the remaining parameters are estimated using only the MOC without requiring an AOC. The formulas to estimate the parameters according to the FP approach in a given OC are the following:

$$\hat{L}_q = -\frac{\bar{\bar{u}}_d + \bar{D}_d \hat{V}_{\text{dead}} - \tilde{R}_0 \bar{\bar{i}}_{d\Theta}}{\bar{\bar{i}}_q \bar{\omega}} \tag{51a}$$

$$\hat{R}' = \frac{\bar{\bar{u}}_d + \bar{D}_d \hat{V}_{\text{dead}} + \tilde{L}_{q0} \bar{\omega} \bar{\bar{i}}_q}{\bar{\bar{i}}_{d\Theta}} \tag{51b}$$

$$\hat{L}_d = \frac{\bar{\bar{u}}_q + \bar{D}_q \hat{V}_{\text{dead}} - \tilde{R}_0 \bar{\bar{i}}_{q\Theta} - \tilde{\psi}_0 \bar{\omega}}{\bar{\bar{i}}_d \bar{\omega}} \tag{51c}$$

$$\hat{\psi} = \frac{\bar{\bar{u}}_q + \bar{D}_q \hat{V}_{\text{dead}} - \tilde{R}_0 \bar{\bar{i}}_{q\Theta} - \tilde{L}_{d0} \bar{\bar{i}}_d \bar{\omega}}{\bar{\omega}}. \tag{51d}$$

The second online non-invasive approach considered is from [40]. This approach exploits a RLS based on the α-β frame voltage functions to overcome the rank deficiency issue without signal injection and AOCs. The forgetting factor (λ) of the RLS has been set equal to 0.99.

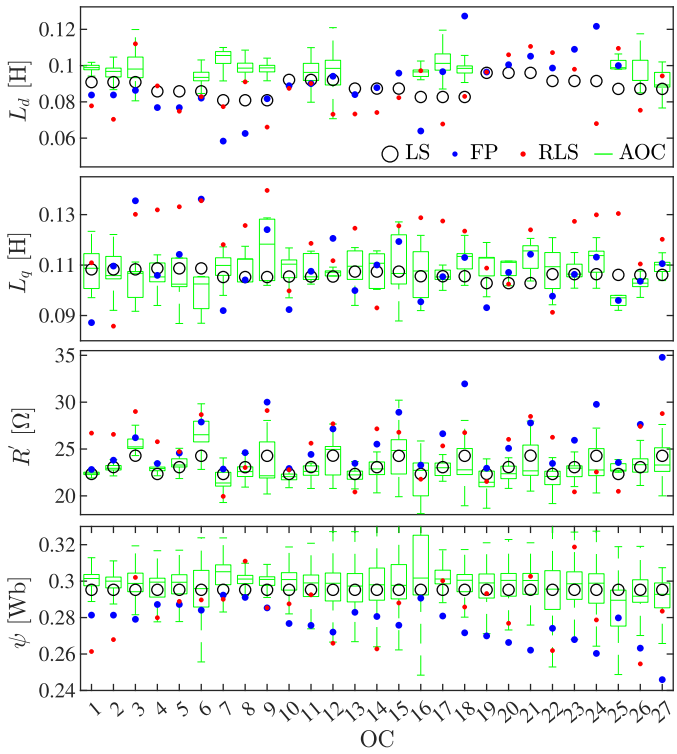

Fig. 14. Comparison between the proposed method and other online noninvasive approaches.

The comparative analysis is reported in Fig. 14, adopting the first hyperparametrization for all the three methods for a fair comparison. In particular, the hyperparameters are used to assign the values of the FPs of the FP method and to initialize the estimations of the RLS method. Concerning the proposed method (denoted as AOC method), the figure reports the statistical analysis of the results obtained when only three additional OCs besides the MOC are available. In other words, the AOC is selected among three OCs (different from the MOC). The three available OCs are chosen considering all the possible combinations among the full dataset. The number of possible combinations when selecting k_s OCs from the dataset is given by

$$N_{\text{comb}} = \frac{27!}{k_s!(27 - k_s)!}. \tag{52}$$

The statistical analysis is presented in terms of boxplots. The central line in the boxes represents the median while the lower and upper edges of the boxes represent the 25th and 75th percentile, respectively. The whiskers represent the minimum and maximum values. The results of the proposed method are not shown for the OCs in which all the estimations have been rejected. The same happens for the two other methods when errors higher than 50% occur.

The figure shows that the proposed approach, even in conditions of data scarcity, produces statistically lower estimation errors than the other two methods for all the parameters. In fact, as summarized in Table V, the MAPEs based on the medians of the estimations obtained using the proposed method

TABLE V
MAPEs [%] OF THE PROPOSED AND OTHER ONLINE NONINVASIVE METHODS ON THE MUT1 DATASET

Method	L_d	L_q	$R^{'}$	ψ
Proposed	13.46	3.61	2.01	1.20
FP	19.45	8.58	11.60	6.35
RLS	18.46	17.05	10.53	6.13

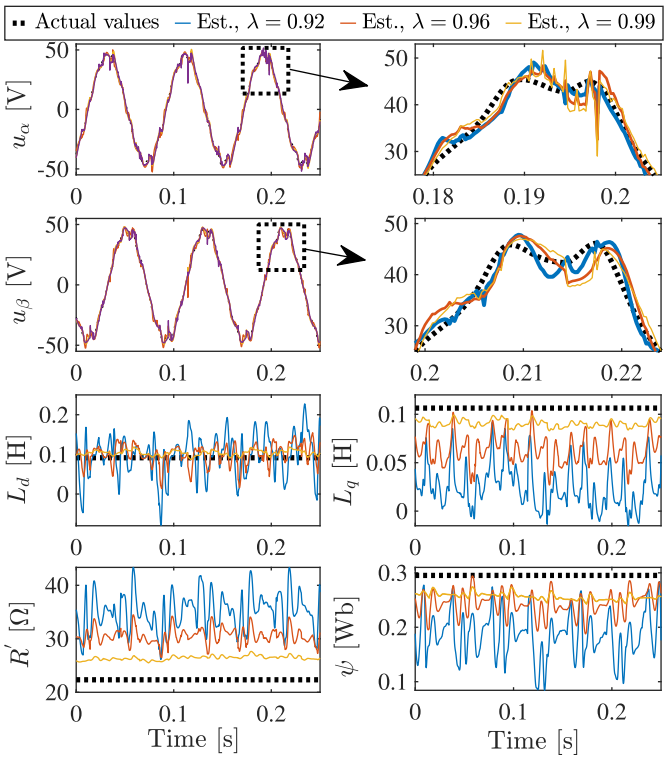

Fig. 15. Performance analysis of the RLS method with different forgetting factors.

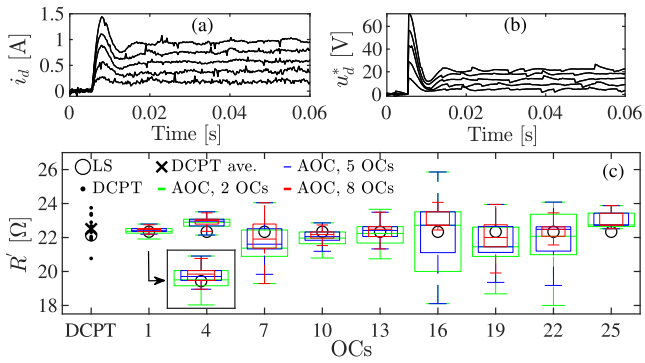

Fig. 16. Comparison between proposed and DCPT method: (a) and (b) d-axis currents and voltage references collected during the DCPT, (c) estimated stator resistance.

TABLE VI
MAPE [%] OF THE PROPOSED AND OTHER OFFLINE METHODS ON THE MUT1 DATSET

Parameter	**MAPE [%] Proposed Method (2, 5, 8 OCs)**	**MAPE [%] Comparison Method**
$R^{'}$	2.05 / 1.41 / 1.28	DCPT: 1.87
L_d	23.77 / 24.18 / 24.17	DVPT: 6.79
L_q	5.93 / 5.48 / 4.97	DVPT: 4.33
ψ	2.09 / 2.01 / 2.00	CQCT: 0.25

are consistently lower than those achieved by the FP and RLS approaches. The main reason behind the lower accuracy of the FP method lies in its sensitivity to parameter variations. On the other hand, the accuracy of the RLS method is largely affected by the value of the forgetting factor, indicating that the estimation problem remains ill-conditioned. This can be clearly seen in Fig. 15 that reports the estimations of the four parameters and of the α-β voltages (u_α, u_β) with different values of the forgetting factor. The parameter estimations are inconsistent, with significant variations depending on the forgetting factor, even if the estimated voltages are comparable throughout the three scenarios and precisely match the real voltages. Consider also that the FP and RLS methods are more vulnerable to errors in the voltages while the proposed method mitigates these errors by properly selecting the AOCs.

D. Comparison With Other Offline Approaches

In this subsection, the proposed parameter estimation method is compared with other two existing offline methods. The first one, presented in [41], is based on the execution of three different tests on the motor to separately estimate the stator resistance, the stator inductances and the rotor flux linkage. The test for estimating the stator resistance is based on the injection of two different d-axis current pulses at zero speed and load, and is hereafter denoted as the double current pulse test (DCPT). The steady-state average values of the d-axis currents and voltage references collected during two different pulses are exploited to estimate the stator resistance. This is a widely adopted approach that allows the compensation of the voltage distortion introduced by the VSI nonlinearity [42], [43]. Fig. 16 shows the comparison between the proposed and DCPT method on the MUT1. Fig. 16(a) and (b) shows the d-axis currents and voltage references during the DCPT. Since a precise rule for the selection of the amplitude of current pulses is not available in the literature, the accuracy of the DCPT method is evaluated considering five different amplitudes of the current pulses in the range [0.2 1]A. Fig. 16(c) shows the estimations obtained by the two methods. The black dots represent the estimations of R' obtained with the DCPT method considering all the possible couples of injected d -axis currents. Meanwhile, the black cross represents the average value of the estimations. The proposed method is evaluated considering as MOCs all the OCs at 150 r/min (the lowest speed in the dataset) to minimize ac effects and provide a proper comparison with DCPT, which estimates the stator resistance at zero speed. In particular, the figure reports the statistic analysis of the estimations obtained when other 2, 5, and 8 OCs are available in addition to the MOCs to select the AOCs. Note that, the 80% of all the possible combinations of OCs in the dataset (depending on the number of available OCs) have been randomly selected and evaluated to produce the statistical analysis for each MOC. Instead, the first row of Table VI summarizes the MAPEs obtained by the proposed

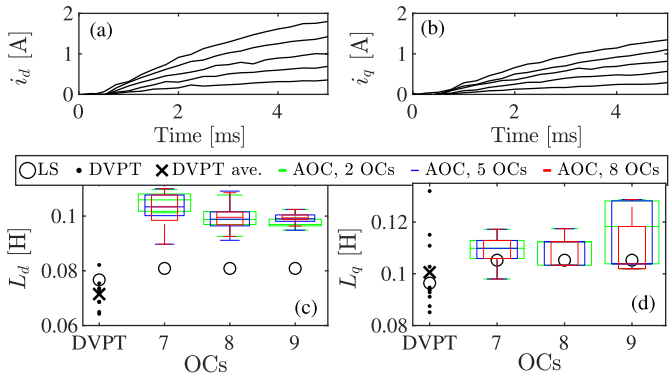

Fig. 17. Comparison between proposed and DVPT method: (a) and (b) dq-axes current responses collected during the DVPT, (c) and (d) estimated dq-axes inductances.

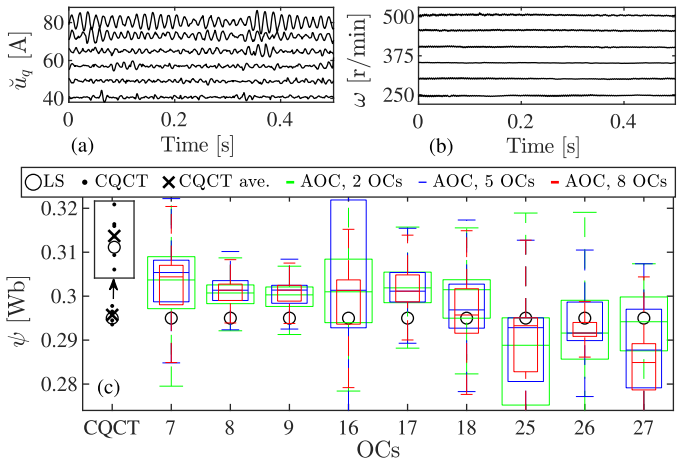

Fig. 18. Comparison between proposed and CQCT method: (a) and (b) q-axis compensated voltage and speed during the CQCT, (c) estimated rotor flux linkage.

method considering the medians of the estimations and by the DCPT. The boxplots show that the accuracy of the proposed method statistically improves with increasing the quantity of available OCs. It can be noticed both a reduction of the errors in the 25th–75th percentile range and of the maximum errors as the number of available OCs increases. This also implies a reduction of the average errors, as shown in Table VI.

In [41], the L_d and L_q are instead estimated through a test in which two different voltage pulses are respectively applied to the d- and q-axis at zero speed and load. The values of the dq-axes currents after a predefined time interval, together with the applied voltage references, are then exploited to estimate the inductances. This method is hereafter denoted as double voltage pulse test (DVPT). In this method, since only the initial part of the current transient is considered to estimate the inductances, the value of the current is low and the saturation effects can be neglected. Furthermore, as in the DCPT, injecting two distinct voltage pulses allows for VSI nonlinearity compensation. Fig. 17 shows the comparison between the proposed and the DVPT method on the MUT1. Fig. 17(a) and (b) shows the dq-axes currents during the DVPT. As for the DCPT, the accuracy of the DVPT method is evaluated considering five different amplitudes of the voltage pulses in the range [10 50]V. As expected, the d-axis current responses are slower compared to the q-axis current since $L_{d0} < L_{q0}$ (see Table II). Fig. 17(c) and (d) shows the estimations of L_d and L_q obtained with the two methods. The black dots represent the estimations obtained with the DVPT method considering all the possible couples of injected voltage pulses. Meanwhile, the black cross represents the average value of the estimations, whose corresponding errors are reported in Table VI. To ensure a fair comparison, the proposed method is evaluated considering as MOCs the three OCs at the lowest dq-axes currents (OCs 7, 8, and 9) to neglect magnetic saturation effects. As in Figs. 16(c), 17(c) and 17(d) report the boxplots related to the proposed method when other 2, 5, and 8 OCs are available in addition to the MOCs. As it can be seen, the DVPT largely outperforms the proposed method in the estimation of L_d whereas the accuracy of the two methods is in the estimation of L_q. The MAPEs considering the medians of the estimations obtained for L_d and L_q are reported in Table VI.

Finally, in [41], the rotor flux linkage is estimated by performing a constant q-axis current control test on the motor unloaded. The steady-state measured q-axis current and voltage reference, speed, and the previously estimated stator resistance are then used to compute the rotor flux linkage. The impact of the VSI nonlinearity is neglected since the motor reaches a high speed at steady state. This method is hereafter denoted as constant q-axis current test (CQCT). Fig. 18 shows the comparison between the proposed and CQCT method on the MUT1. Fig. 18(a) and (b) shows the q-axis voltages and mechanical rotor speed at steady state collected during the CQCT. Six different test have been performed with the speed in the range [250 500]r/min. Fig. 18(c) shows the estimations of ψ obtained with the two methods. The black dots represent the estimations obtained in the six tests while the black cross represents the average estimated value, whose corresponding error is reported in Table VI. Since the CQCT is a method at zero d-axis current, the proposed method is evaluated in the OCs having the lowest d-axis current, i.e., OCs 7, 8, 9, 16, 17, 18, 25, 26, and 27. The figure shows the boxplots generated using the same logic as before. Also, in this case, it is clear that the errors in the 25th–75th percentile range and the maximum errors decrease as the number of available OCs increases. Similarly, the MAPEs obtained considering the medians of the estimations decrease as the available OCs increase, as reported in Table VI.

As shown in Table VI, a comparison of the MAPEs indicates that the dedicated test-based approaches (DCPT, DVPT, and CQCT) generally achieve greater estimation accuracy than the proposed method. This is clearly owing to the experiments being run in controlled OCs, which favor parameter estimation by avoiding parameter coupling and errors induced by VSI nonlinearity. Unfortunately, these experiments are time-consuming and require the disconnection of the motor from its load. Additionally, the DCPT and DVPT methods allow to estimate the stator resistance and inductances only in limited operating ranges of the motor and cannot provide information on parameter variations. On the other hand, the proposed method, even with

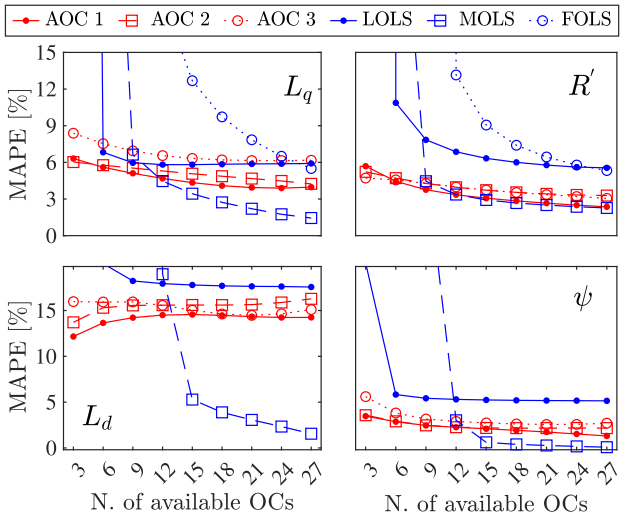

Fig. 19. Comparison between proposed and LS method under data scarcity on MUT1.

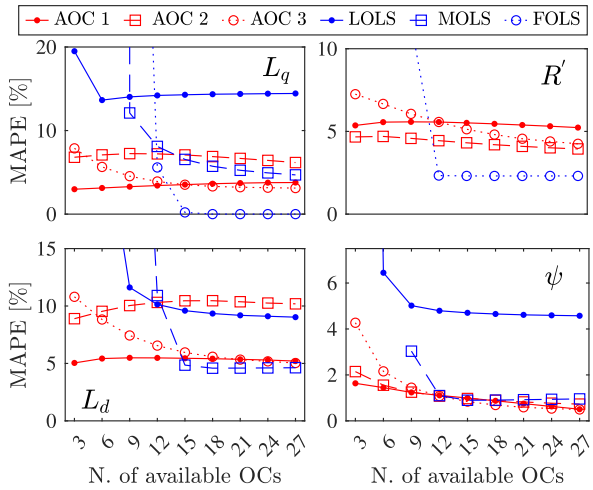

Fig. 20. Comparison between proposed and LS method under data scarcity on MUT2.

lower accuracy, allows estimation of the parameters across the entire motor operating range, avoiding the execution of dedicated tests, motor downtimes and load disconnection. It must be also remarked that statistically the accuracy of the proposed method improves with the number of available OCs. This is a noteworthy result since it demonstrates how the proposed algorithm efficiently leverages the availability of additional data to select better AOCs.

The second offline method considered is the decoupled LS implemented with three models featuring different orders. The full order model (FOLS) is based on (49), while the medium-order (MOLS) is based on

$$\begin{cases} x_1 &= R_0 \bar{i}_{d\Theta} + k_R \frac{\bar{\omega}^2 \bar{i}_{d\Theta}}{(1+\alpha(T_s-20))^{1.5}} + \bar{D}_d V_{\text{dead}} \\ x_2 &= R_0 \bar{i}_{q\Theta} + k_R \frac{\bar{\omega}^2 \bar{i}_{q\Theta}}{(1+\alpha(T_s-20))^{1.5}} + \bar{D}_q V_{\text{dead}} \\ y_1 &= (L_{q0} + \alpha_{q1} i_d + \alpha_{q2} i_q) i_q \\ y_2 &= (L_{d0} + \alpha_{d1} i_d + \alpha_{d2} i_q) i_d + \psi_0 \end{cases}. \quad (53)$$

Finally, the low-order model (LOLS) is based on the following simple set of equations:

$$\begin{cases} x_1 &= R_0 \bar{i}_{d\Theta} + \bar{D}_d V_{\text{dead}} \\ x_2 &= R_0 \bar{i}_{q\Theta} + \bar{D}_q V_{\text{dead}} \\ y_1 &= L_{q0} i_q \\ y_2 &= L_{d0} i_d + \psi_0 \end{cases}. \quad (54)$$

Differently from the proposed method, the decoupled LS approach, rather than using only 2 OCs, simultaneously exploits all the available OCs to estimate the motor parameters.

Figs. 19 and 20 compare the MAPEs of the proposed and decoupled LS method, respectively, on MUT1 and MUT2 changing the quantity of available OCs. Note that the MAPEs are computed with respect to the reference values obtained using the LS method applied to the full datasets consisting of 48 and 75 OCs respectively. The results of the proposed method are reported for the three hyperparametrizations in Table III.

As in the previous analysis, the available OCs are randomly selected. In particular, denoting with k_s the number of OCs to be selected, for $k_s \in [2\ \ 6]$ and $k_s \in [22\ \ 27]$, a number of combinations equal to $N_{\text{comb}} \cdot 4/5$ were analyzed, whereas for the other values of k_s, $2.5 \cdot 10^5$ combinations were analyzed. The results of the FOLS are not visible for L_d and ψ due to excessive errors. As it can be seen, in most cases the accuracy of the proposed method statistically increases with the number of available OCs, confirming the trend observed in the previous analysis. Similar but more pronounced descending trends are also evident for the LS method even if the accuracy of the LOLS stops improving after just a few available OCs (between 9 and 12), whereas the accuracy of the MOLS and FOLS generally continues to improve even after 15 available OCs. When few OCs are available (e.g., 3–9 OCs), for both motors, the proposed technique clearly outperforms the LS, regardless of model order or hyperparameter choices. It is also worth noting that there are no significant discrepancies between the three distinct hyperparametrizations, further emphasizing the robustness of the suggested method. Finally, the errors obtained with the LS technique confirm that L_d is the most challenging parameter to estimate for both the MUTs. In fact, the figure shows that more than 15 OCs are statistically required to ensure an error lower than 5% by the MOLS.

E. Tuning of Current Controllers Using Estimated Parameters

To conclude the validation of the proposed method, the performance of the PI current controllers tuned with the estimated parameters is evaluated on the MUT2. For the tuning of the PI regulators, the modulus optimum (MO) criterion is applied under the assumption of a total closed-loop delay equal to $2T_c$. This delay arises from the digital implementation of the regulators, the PWM VSI delay, and the analog-to-digital conversion of the measured phase currents. Under these assumptions, the following formulas are adopted for the tuning of the regulators

$$k_{pd} = \hat{L}_d/(4T_c),\ \ k_{pq} = \hat{L}_q/(4T_c),\ \ k_{id} = k_{iq} = \hat{R}/(4T_c) \quad (55)$$

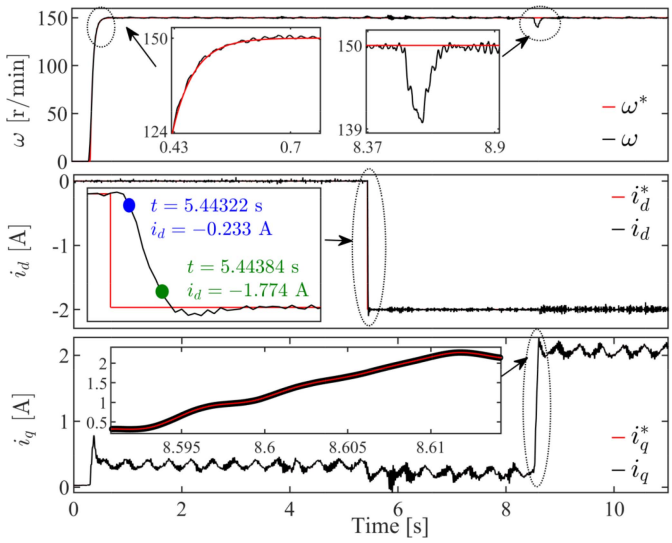

Fig. 21. Evaluation of PI current controllers tuned with the estimated parameters on MUT2.

where k_{pd} and k_{pq} are the proportional gains while k_{id} and k_{iq} are the integral gains. The feedforward compensation of the back electromotive force in the q-axis ($\hat{\psi}\,\omega$) is also implemented to enhance the static performance.

Fig. 21 shows the MUT2 speed and dq-axis current waveforms during a short test using the parameter estimation results reported in Fig. 11 obtained in OC 1 (first hyperparametrization). In this test, the speed is regulated by an external closed-loop PI speed controller, which provides the q-axis current reference i_q^*, while the d-axis current reference i_d^* is arbitrarily varied. At $t = 5.5$ s, the d-axis current reference is set to $i_d^* = -2$ A, and at $t = 8.5$ s a $1\,\mathrm{N}\cdot\mathrm{m}$ load torque step is applied. As it can be seen, the speed reference ω^*, filtered with a smoothing filter, is precisely tracked by the actual motor speed during the initial transient. In addition, the motor rapidly recovers the reference speed after the application of the load torque step with a maximum error of -10 r/min. Concerning the d-axis current, it can be observed that the step response has a low overshoot ($\approx 7\%$) and a short 10% -90% rising time ($\approx 5T_c$), which are considered acceptable. The steady-state tracking error is practically zero. Finally, the q-axis current accurately follows the reference set by the speed regulator both during motor start-up and after the application of the load torque step. A slight reduction in i_q after the d-axis current step can also be observed. This is due to the automatic adjustment of i_q^* by the speed regulator, which compensates for the reluctance torque generated by the increase in i_d. Overall, it can be concluded that the standard PI regulators tuned using the estimated parameters ensure acceptable static and dynamic performance.

VI. Conclusion

This work has proposed an automated noninvasive parameter estimation approach for PMSMs controlled with nonzero d-axis current. Unlike existing approaches in the literature, the proposed method is specifically designed for application scenarios where custom signal injection and dedicated test campaigns on instrumented laboratory test rigs are not feasible. This makes it particularly suitable for large-scale deployment in industrial environments, as it avoids machine downtime, reduces human effort, and eliminates the need for dedicated instrumentation.

The performance of the proposed method has been statistically evaluated and benchmarked against existing approaches from the literature under conditions of limited and uncertain measurement data availability. The salient findings can be summarized as follows.

1) The designed algorithm is able to automatically reject estimations affected by high errors.
2) The accuracy of the algorithm statistically improves as data availability increases.
3) The proposed method is weakly sensitive to its hyperparameters, demonstrating robustness to uncertainties in motor information.
4) The proposed method outperforms existing noninvasive methods under data-scarce conditions.

References

[1] A. Floris, M. Porru, A. Damiano, and A. Serpi, "Energy management and control system design of an integrated flywheel energy storage system for residential users," *Appl. Sci.*, vol. 11, no. 10, 2021, Art. no. 4615.
[2] E. Brescia, M. Palmieri, P. R. Massenio, G. L. Cascella, and F. Cupertino, "Cogging torque suppression of modular permanent magnet machines using a semi-analytical approach and artificial intelligence," *IEEE Access*, vol. 11, pp. 39405–39417, 2023.
[3] V. Madonna, P. Giangrande, L. Lusuardi, A. Cavallini, C. Gerada, and M. Galea, "Thermal overload and insulation aging of short duty cycle, aerospace motors," *IEEE Trans. Ind. Electron.*, vol. 67, no. 4, pp. 2618–2629, Apr. 2020.
[4] M. Porru, A. Serpi, A. Floris, and A. Damiano, "Modelling and real-time simulations of electric propulsion systems," in *Proc. Int. Conf. Elect. Syst. Aircraft, Railway, Ship Propulsion Road Veh. Int. Transp. Electrific. Conf.*, 2016, pp. 1–6.
[5] M. A. Hamida, J. De Leon, A. Glumineau, and R. Boisliveau, "An adaptive interconnected observer for sensorless control of PM synchronous motors with online parameter identification," *IEEE Trans. Ind. Electron.*, vol. 60, no. 2, pp. 739–748, Feb. 2013.
[6] O. C. Kivanc and S. B. Ozturk, "Sensorless PMSM drive based on stator feedforward voltage estimation improved with MRAS multiparameter estimation," *IEEE/ASME Trans. Mechatron.*, vol. 23, no. 3, pp. 1326–1337, Jun. 2018.
[7] P. R. Massenio, M. Tipaldi, G. Rizzello, E. Brescia, G. L. Cascella, and D. Naso, "Gain-scheduled structured control in DC microgrids," *IEEE Trans. Control Syst. Technol.*, vol. 31, no. 6, pp. 2571–2583, Nov. 2023.
[8] X. Wang et al., "Optimization-based parameter estimation for PMSMs under unified observable conditions," *IEEE Trans. Power Electron.*, vol. 39, no. 2, pp. 2632–2643, Feb. 2024.
[9] Y. Zhang, M. Zhou, C. Zhang, A. Shen, and L. Bing, "Identification of PMSM parameters with time-error compensated based on contractile factor antipredator PSO," *IEEE Trans. Transp. Electrif.*, vol. 10, no. 2, pp. 4006–4017, Jun. 2024.
[10] W. Feng, W. Zhang, and S. Huang, "A novel parameter estimation method for PMSM by using chaotic particle swarm optimization with dynamic self-optimization," *IEEE Trans. Veh. Technol.*, vol. 72, no. 7, pp. 8424–8432, Jul. 2023.
[11] C. Lian, F. Xiao, J. Liu, and S. Gao, "Parameter and vsi nonlinearity hybrid estimation for PMSM drives based on recursive least square," *IEEE Trans. Transp. Electrif.*, vol. 9, no. 2, pp. 2195–2206, Jun. 2023.
[12] Z. Q. Zhu, D. Liang, and K. Liu, "Online parameter estimation for permanent magnet synchronous machines: An overview," *IEEE Access*, vol. 9, pp. 59059–59084, 2021.
[13] Y. Inoue, Y. Kawaguchi, S. Morimoto, and M. Sanada, "Performance improvement of sensorless IPMSM drives in a low-speed region using online parameter identification," *IEEE Trans. Ind. Appl.*, vol. 47, no. 2, pp. 798–804, Mar./Apr. 2011.

[14] X. Li and R. Kennel, "General formulation of Kalman-filter-based online parameter identification methods for VSI-fed PMSM," *IEEE Trans. Ind. Electron.*, vol. 68, no. 4, pp. 2856–2864, Apr. 2021.
[15] S. Liu et al., "Virtual-axis injection based online parameter identification of PMSM considering cross coupling and saturation effects," *IEEE Trans. Power Electron.*, vol. 38, no. 5, pp. 5791–5802, May 2023.
[16] K. Yu and Z. Wang, "Online decoupled multi-parameter identification of dual three-phase IPMSM under position-offset and HF signal injection," *IEEE Trans.Ind. Electron.*, vol. 71, no. 4, pp. 3429–3440, Apr. 2024.
[17] Y. Li, C. Wang, J. Hang, and S. Ding, "Parallel iron loss resistance equivalent impedance model method for online full parameters identification of PMSM," *IEEE J. Emerg. Sel. Topics Power Electron.*, vol. 13, no. 2, pp. 1783–1791, Apr. 2025.
[18] Q. Wang, X. Zhao, P. Yang, W. Hua, and G. Buja, "Effects of triangular wave injection and current differential terms on multiparameter identification for PMSM," *IEEE Trans. Power Electron.*, vol. 39, no. 3, pp. 2943–2947, Mar. 2024.
[19] Y. Wang, Y. Xu, and J. Zou, "Online multiparameter identification method for sensorless control of SPMSM," *IEEE Trans. Power Electron.*, vol. 35, no. 10, pp. 10601–10613, Oct. 2020.
[20] X. Yang, J. Zhan, Y. Shen, P. Liu, L. Guo, and Z. Zhang, "Parameter identification for SPMSM based on a superior ROA," *IEEE Trans. Power Electron.*, vol. 40, no. 6, pp. 7615–7627, Jun. 2025.
[21] Y. Zhang, S. Li, W. Yi, Y. Yang, K. Cao, and B. Luo, "A robust model predictive current closed-loop control with parameter estimation strategy based on immune chaotic antipredator PSO for PMSM," *IEEE Trans. Power Electron.*, vol. 40, no. 1, pp. 1836–1848, Jan. 2025.
[22] Z. Tong et al., "Dual position offset injection based multi-parameter decoupled estimation of PMSM considering signal injection induced inductance variation," *IEEE Trans. Ind. Appl.*, vol. 60, no. 5, pp. 6913–6922, Sep./Oct., 2024.
[23] P. Wang, Z. Q. Zhu, and D. Liang, "Improved position-offset based online parameter estimation of PMSMs under constant and variable speed operations," *IEEE Trans. Energy Convers.*, vol. 39, no. 2, pp. 1325–1340, Jun. 2024.
[24] K. Yu, Z. Wang, X. Wang, and Z. Zou, "An online flux estimation for dual three-phase SPMSM drives using position-offset injection," *IEEE Trans. Power Electron.*, vol. 36, no. 10, pp. 11606–11617, Oct. 2021.
[25] Q. Wang, G. Zhang, G. Wang, C. Li, and D. Xu, "Offline parameter self-learning method for general-purpose PMSM drives with estimation error compensation," *IEEE Trans. Power Electron.*, vol. 34, no. 11, pp. 11103–11115, Nov. 2019.
[26] G. Lu, J. Su, G. Yang, and F. Liu, "Offline parameter self-learning method for low-impedance dual three-phase PMSMs: Addressing ac losses and inverter nonlinearity," *IEEE J. Emerg. Sel. Topics Power Electron.*, vol. 12, no. 3, pp. 2730–2743, Jun. 2024.
[27] C. Lai, G. Feng, Z. Li, and N. C. Kar, "Computation-efficient decoupled multiparameter estimation of PMSMs from massive redundant measurements," *IEEE Trans. Power Electron.*, vol. 35, no. 10, pp. 10729–10740, Oct. 2020.
[28] K. Huang, B. Ding, C. Lai, G. Feng, and N. C. Kar, "PMSM combination modeling for multiparameter estimation using Bayesian learning with inverter distortion cancellation and temperature compensation," *IEEE Trans. Energy Convers.*, vol. 38, no. 2, pp. 1004–1015, Jun. 2023.
[29] G. Zanuso, V. Fodor, L. Peretti, and O. Wallmark, "Networked electric drives in the industry 4.0," in *Proc. IEEE 21st Int. Conf. Elect. Mach. Syst.*, 2018, pp. 724–729.
[30] E. Brescia, P. R. Massenio, M. D. Nardo, G. L. Cascella, C. Gerada, and F. Cupertino, "Nonintrusive parameter identification of IoT-embedded isotropic PMSM drives," *IEEE J. Emerg. Sel. Topics Power Electron.*, vol. 11, no. 5, pp. 5195–5207, Oct. 2023.
[31] E. Brescia, P. R. Massenio, M. D. Nardo, G. L. Cascella, C. Gerada, and F. Cupertino, "Parameter estimation of isotropic PMSMs based on multiple steady-state measurements collected during regular operations," *IEEE Trans. Energy Convers.*, vol. 39, no. 1, pp. 130–145, Mar. 2024.
[32] A. V. Udovichenko, S. V. Brovanov, E. V. Grishanov, and S. M. Stennikova, "A five-level converter in a three-level mode for common-mode leakage current suppression in PV-generation systems," *Electronics*, vol. 10, no. 19, 2021, Art. no. 2382.
[33] G. Feng, C. Lai, K. Mukherjee, and N. C. Kar, "Current injection-based online parameter and VSI nonlinearity estimation for PMSM drives using current and voltage DC components," *IEEE Trans. Transp. Electrif.*, vol. 2, no. 2, pp. 119–128, Jun. 2016.
[34] W. Deng, C. Xia, Y. Yan, Q. Geng, and T. Shi, "Online multiparameter identification of surface-mounted PMSM considering inverter disturbance voltage," *IEEE Trans. Energy Convers.*, vol. 32, no. 1, pp. 202–212, Mar. 2017.
[35] T. Zwerger and P. Mercorelli, "Backward extended Kalman filter to estimate and adaptively control a PMSM in saturation conditions," *IEEE J. Emerg. Sel. Topics Ind. Electron*, vol. 5, no. 2, pp. 462–474, Apr. 2024.
[36] Q. Wang et al., "An offline parameter self-learning method considering inverter nonlinearity with zero-axis voltage," *IEEE Trans. Power Electron.*, vol. 36, no. 12, pp. 14098–14109, Dec. 2021.
[37] R. Wrobel, A. Mlot, and P. H. Mellor, "Contribution of end-winding proximity losses to temperature variation in electromagnetic devices," *IEEE Trans. Ind. Electron.*, vol. 59, no. 2, pp. 848–857, Feb. 2012.
[38] J.-W. Chin, K.-S. Cha, J.-C. Park, D.-M. Kim, J.-P. Hong, and M.-S. Lim, "Investigation of ac resistance on winding conductors in slot according to strands configuration," *IEEE Trans. Ind. Appl.*, vol. 57, no. 1, pp. 316–326, Jan./Feb. 2021.
[39] K. Liu and Z. Q. Zhu, "Online estimation of the rotor flux linkage and voltage-source inverter nonlinearity in permanent magnet synchronous machine drives," *IEEE Trans. Power Electron.*, vol. 29, no. 1, pp. 418–427, Jan. 2014.
[40] Y. Yu et al., "Full parameter estimation for permanent magnet synchronous motors," *IEEE Trans. Ind. Electron.*, vol. 69, no. 5, pp. 4376–4386, May 2022.
[41] S.-M. Yang and K.-W. Lin, "Automatic control loop tuning for permanent-magnet ac servo motor drives," *IEEE Trans. Ind. Electron.*, vol. 63, no. 3, pp. 1499–1506, Mar. 2016.
[42] A. Dianov, "An algorithm for offline measurement of motor stator resistance and voltage drop across inverter switches for washing machine drives," *IEEE J. Emerg. Sel. Topics Power Electron.*, vol. 10, no. 5, pp. 5798–5808, Oct. 2022.
[43] S. A. Odhano, P. Giangrande, R. I. Bojoi, and C. Gerada, "Self-commissioning of interior permanent- magnet synchronous motor drives with high-frequency current injection," *IEEE Trans. Ind. Appl.*, vol. 50, no. 5, pp. 3295–3303, Sep./Oct. 2014.

Elia Brescia received the M.Sc. (*Hons*.) and Ph.D. degrees in electrical engineering from the Polytechnic University of Bari, Bari, Italy, in 2018, and 2022, respectively.

He is currently an Assistant Professor of electric drives with the Polytechnic University of Bari. He is the coauthor of more than 25 papers published in proceedings of international conferences or international archival journals and holds a patent as the inventor of a noninvasive procedure for parameter identification of permanent magnet synchronous machines. His research interests include design, control, analysis and monitoring of electrical machines and power systems.

Luigi Pio Savastio (Graduate Student Member, IEEE) received the the M.Sc. degree in electrical engineering, in 2023, from Polytechnic University of Bari, Italy, where he is currently working toward the Ph.D. in electrical and information engineering.

His research interests include control and parameter estimation of permanent magnet synchronous motors and smart grids management with integration of multivector energy resources.

Mauro Di Nardo (Member, IEEE) received the M.Sc. (*Hons*.) degree in electrical engineering from the Polytechnic University of Bari, Italy, in 2012, and the Ph.D. degree in electrical machine design from the University of Nottingham, U.K., in 2017.

From 2017 to 2019, he was with the AROL spa leading the R&D team focusing on electrical drives design for mechatronics applications. Between 2019 and 2023, he was with the Power Electronics and Machine Control Group of the University of Nottingham as a Senior Research Fellow. He is currently an Assistant Professor in electrical machine and drives with the Polytechnic University of Bari, Italy.

Dr. Nardo serves as an Associate Editor for the IEEE OPEN JOURNAL OF INDUSTRY APPLICATIONS and IEEE TRANSACTIONS ON ENERGY CONVERSION. His main research interests include the modeling, design optimizations and testing of permanent magnet, synchronous reluctance, and induction machines for automotive, industrial and aerospace applications as well as niche machine topologies such as bearingless, homopolar and hysteresis motors

Giuseppe Leonardo Cascella (Member, IEEE) received the M.Sc. degree with honors, in 2001, and the Ph.D. degree in electrical engineering, in 2005, both from the Polytechnic University of Bari, Italy.

He is currently an Assistant Professor of Electric Drives with Polytechnic University of Bari. He has authored or coauthored 70+ peer-reviewed scientific papers on industry 4.0 and AI applications, has been the coordinator of 30+ R&D industrial projects and received the following awards: 2018 AWS Activate Builder, "Cloud Data Analytics for Energy Efficiency", Amazon Web Services, 2018; best experiment in Open Call 2, BEinCPPS, H2020, EU funded, project 680633, 2018; "SmartSupervisor for Cognitive Energy Efficiency", A&T award for the best innovative i4.0 solution, 2017.

Dr. Cascella won two EU Marie Curie Fellowships at Nottingham University (U.K.) and the University of Malta. He completed his Postdoctoral Research project (2008) "Adaptive Memetic Algorithms for Electric Drives". He is the founder (2015) and CEO of Idea75.it. He is a member of the Italian National Order of Engineers.

Francesco Cupertino (Senior Member, IEEE) received the Laurea and Ph.D. degrees in electrical engineering from the Politecnico di Bari, Italy, in 1997 and 2001, respectively.

Since 2001, he has been with the Department of Electrical and Information Engineering at the same university, where he is currently a Full Professor of Converters, Electrical Machines, and Drives. He has promoted the creation of several joint public-private laboratories with leading companies, including AVIO Aero (GE Aerospace), AROL, and Molino Casillo, as well as the BINP-Business Innovation in PoliBA incubator. From 2019 to 2025, he served as Rector of the Politecnico di Bari. He is currently Chairman of the NEST Foundation (Network 4 Energy Sustainable Transition), and Italy's representative in the OECD Working Group on Research Security and Integrity. He has authored or coauthored more than 200 scientific papers in these fields. His research interests include the design and control of synchronous electrical machines, motion control for high-performance drives, applications of computational intelligence to control systems, and sensorless control of ac electric drives.